2016

IMPROVING THE CAPACITY, DURABILITY AND STABILITY OF LITHIUM-ION BATTERIES BY INTERPHASE ENGINEERING

Qinglin Zhang
University of Kentucky, qinglinzhang@uky.edu
Digital Object Identifier: http://dx.doi.org/10.13023/ETD.2016.170

STUDENT AGREEMENT:

I represent that my thesis or dissertation and abstract are my original work. Proper attribution has been given to all outside sources. I understand that I am solely responsible for obtaining any needed copyright permissions. I have obtained needed written permission statement(s) from the owner(s) of each third-party copyrighted matter to be included in my work, allowing electronic distribution (if such use is not permitted by the fair use doctrine) which will be submitted to UKnowledge as Additional File.

I hereby grant to The University of Kentucky and its agents the irrevocable, non-exclusive, and royalty-free license to archive and make accessible my work in whole or in part in all forms of media, now or hereafter known. I agree that the document mentioned above may be made available immediately for worldwide access unless an embargo applies.

I retain all other ownership rights to the copyright of my work. I also retain the right to use in future works (such as articles or books) all or part of my work. I understand that I am free to register the copyright to my work.

REVIEW, APPROVAL AND ACCEPTANCE

The document mentioned above has been reviewed and accepted by the student's advisor, on behalf of the advisory committee, and by the Director of Graduate Studies (DGS), on behalf of the program; we verify that this is the final, approved version of the student's thesis including all changes required by the advisory committee. The undersigned agree to abide by the statements above.

Qinglin Zhang, Student

Dr. Yang-Tse Cheng, Major Professor

Dr. Thomas Dziubla, Director of Graduate Studies

IMPROVING THE CAPACITY, DURABILITY AND STABILITY OF LITHIUM-ION BATTERIES BY INTERPHASE ENGINEERING

DISSERTATION

A dissertation submitted in partial fulfillment of the requirements for the degree of Doctor of Philosophy in the College of Engineering at the University of Kentucky

By

Qinglin Zhang

Lexington, Kentucky, United States

Director: Dr. Yang-Tse Cheng, Professor of Materials Engineering,
University of Kentucky

2016

ABSTRACT OF DISSERTATION

IMPROVING THE CAPACITY, DURABILITY AND STABILITY OF LITHIUM-ION BATTERIES BY INTERPHASE ENGINEERING

This dissertation is focus on the study of solid-electrolyte interphases (SEIs) on advanced lithium ion battery (LIB) anodes. The purposes of this dissertation are to a) develop a methodology to study the properties of SEIs; and b) provide guidelines for designing engineered SEIs. The general knowledge gained through this research will be beneficial for the entire battery research community.

KEYWORDS: Li-ion Batteries, Solid-Electrolyte Interphase, Surface Coatings, Mechanical Properties, Engineered SEI

ACKNOWLEDGEMENT

First of all, I would like to acknowledge to my Ph.D. advisor, Dr. Yang-Tse Cheng for his continuous support and help on my academic research, and career development. Dr. Cheng guided me with a very efficient way of exploring new knowledge, conducting research and providing solutions. Drs. Xingcheng Xiao and Mark W. Verbrugge from General Motors have also contributed a lot of their talents to my research.

I am also grateful to my committee members, Drs. T. John Balk, Stephen Rankin, Doo Young Kim and Xingcheng Xiao for their efforts and suggestions on my dissertation.

I would like to thank my lab mates and previous group members, Dr. Juchuan Li, Dr. Rutooj D. Deshpande, Dr. Ilona Hoffmann, Jie Pan, Jiagang Xu, Tao Chen, Alshroofy Mohanad, Baleegh Alobaid, Yikai Wang, Long Zhang, Jiazhi Hu, for their support and help on my research. We worked together, and made our group a prefect and fun place to work productively.

General Motors R&D Center is also acknowledged. GM offered me four times of summer internships, which allowed me to access their facilities and get to know more about the current status and future needs of the industry. Researchers at GM are greatly appreciated, including Drs. Peng Lu, Steve Harris (now at LBNL), Weidong Zhou (now at UT-Austin), Yue Qi (now at Michigan State University), Meng Jiang and Yan Wu, Mei Cai for their guidance and support.

I would also like to thank the co-authors of my publications. I enjoyed working and discussing together with them.

The funding agencies are also greatly acknowledged, including National Science Foundation, Department of Energy, and General Motors.

Finally, I would like to thank my parents and my love for their unselfish support.

TABLE OF CONTENTS

LIST OF TABLES

LIST OF FIGURES

Chapter 1. Introduction

Traditionally, energy **generation** and **transmission/distribution** are the two major components before energy utilization. For example, the electricity is generated by the gas turbines, and distributed through transmission lines to substations, then delivered at the end users. Usually, the electric power stations operate based on the demands. Another example is the traditional vehicles with internal combustion engines, the energy in gasoline can be converted by the engine to the mechanical motion, then transmitted to the wheels to drive the vehicles.

However, there is a huge amount of energy waste due to the mismatch between the energy supplies and the demands, especially when considering the instability of renewable energy generation. For example, solar energy stations produce most energy during 1 to 3 PM of the day, but the high demands are usually after 4PM daily. One way to help balancing fluctuations in supply and demand is using energy storage systems. According to the Environmental Protection Agency (EPA) and the Department of Energy (DOE), in the United States, 95% of the electricity stored in pumped hydro stations. However, pumped hydro requires quite a lot of space, or certain terrains, making it impossible to be built in the big cities, such as New York City. There are urgent demands for smaller energy storage systems with higher energy density. Electrochemical energy storage systems can meet these requirements.

Meanwhile, there are increasing demands for improving the fuel efficiency of vehicles. More customers are willing to buy vehicles with higher mileage per gallon to save the fuel cost and reduce the carbon footprint. Hence, automobile manufacturers changed their products to meet the customers' requirements. In addition, government regulations also play an important role in promoting the fuel efficiency. Vehicle electrification is one of the most accepted strategies. Hybrid or plug-in electrical vehicles may be considered as energy storage systems connected to the smart grid.

The consumer electronics market is another example. After SONY® first commercialized them in portable electronic devices in 1991, lithium ion batteries (LIBs) have been used in portable electronic devices for more than 25 years, replacing Ni-metal hydride batteries and dominating the market. Today, electronic devices are equipped with ever larger screens, more powerful processors, and faster network capability, while becoming smaller and lighter. All these features require advanced batteries.

With the growing demands in so many fields, there is a significant amount of research efforts devoted to LIBs to develop battery cells with higher energy density, longer cycle life, and lower cost. In order to achieve these goals, research communities are exploring new electrode materials with new chemistry. For example, on the negative electrode material (or anode) side, silicon-based materials attract much attention. Si electrode has the highest theoretical capacity of 3600 mAh/g by forming $Li_{4.4}Si$ alloys. Moreover, elemental Si is the second most abundant element in the earth crust, which makes is possible to be low cost. However, the Si electrode material swells during Li insertion, causing severe degradation. The stress generated by the 300% volume change causes cracks in the electrode, hence prohibits the formation of stable solid-electrolyte interphase (SEI), leading to low cycling efficiency (or Columbic efficiency).

In this dissertation, we focus on the study of solid-electrolyte interphase on advanced LIB anodes. The purposes of this dissertation are to a) develop a methodology to study the properties of solid-electrolyte interphase; and b) provide guidelines for designing engineered solid-electrolyte interphase. The general knowledge gained through this research will be beneficial for the entire battery research community.

Chapter 1 gives a brief introduction on the motivation of the research. Chapter 2 provides a brief background about LIBs and solid-electrolyte interphase. Chapter 3 studies the naturally formed solid-electrolyte interphase, and revels the relationship between the properties of solid-electrolyte interphase and the impact on cycle efficiency and battery performances. Chapter 4 describes a simple way of determining the elastic properties of ultra-thin artificial solid-electrolyte interphase. Based on the knowledge learned from the naturally formed SEI, we identified two critical components in solid-electrolyte interphase. With a further understanding of the synergetic effects between

these components, in Chapter 5, we designed several artificial solid-electrolyte interphases with high ionic transport and reduced electrolyte decomposition. In Chapter 6, we demonstrated a chemically stable artificial solid-electrolyte interphase. The last Chapter concludes the dissertation and proposes possible future research directions.

Chapter 2. Backgrounds

2.1 Lithium-ion Batteries

Lithium-ion batteries (LIBs) store electrical energy as chemical energy. A typical LIB cell contains a transition metal oxide cathode, a porous polymer separator filled with organic electrolyte, and a carbonaceous anode. In the cell, Li ions move between positive electrode (cathode) and negative electrode (anode) through the electrolyte, while electrons move between two electrodes in the outer circuit. During this process, the chemical potential changes. The chemical potential difference determines the measured voltage between two electrodes.

The positive electrode is generally composed of transition metal oxides, such as $LiCoO_2$ (layered structure),[1, 2] $LiFePO_4$ (olivine-type structure) [3-5] and $LiMn_2O_4$ (spinel structure). [6, 7] The negative electrode is generally composed of different forms of carbon materials (graphite, hard carbon, porous carbon, etc.). [8, 9]

The polymer separator blocks the two electrodes from short, and reduces the self-discharge. Usually the separator is a tri-layer sandwich-like structure. The polyethylene (PE) is sandwiched between two polypropylene (PP) layers. The thickness is around 20 μm. [10]

The organic electrolyte is a liquid solution in commercial LIBs. The solution contains lithium salts, such as $LiPF_6$ or $LiBF_4$, with organic solvents, such as ethylene carbonate (EC), dimethyl carbonate (DMC) and diethyl carbonate (DEC), or a combination of two or more. [11, 12]

2.2 Solid-Electrolyte Interphase

Both terms of solid-electrolyte interphase and solid-electrolyte interface are used in the literature. In this dissertation, solid-electrolyte **interphase** will be referred to as SEI.

SEI was first named by Peled in 1979.[13, 14] A SEI layer is typically on the order of ten nanometer in thickness.

SEI is a passivation layer formed on the electrode surface (mainly on the negative electrode), as a result of electrolyte reduction. A stable SEI can effectively protect the electrode from further decomposition of the electrolyte. Usually, SEI contains multiple Li salts, and several polymeric species. The formation of SEI is a Li consuming process, which causes permanent Li loss in the system (as shown in Figure 2.1). The amount of Li is limited in a Li-ion cell. Due to its good air stability, Li is originally stored in the cathode side, in the form of metal oxides. During the formation cycle, Li transports though the electrolyte from cathode to anode, while SEI is formed on the anode surface. On carbon-based electrodes, such as graphite, once SEI is formed during the formation cycle, it barely changes, and acts as a stable protective layer on the electrode. However, for advanced electrode materials with greater storage capability of Li, such as Si-based anodes, the volume changes dramatically during the cycling, which leads to unstable SEI. When SEI or electrode particles break during the cycling, there will be additional electrolyte reduction to form new SEI, consuming Li and electrolyte continuously. Figure 2.2 illustrates two cases with stable and unstable SEI formation, respectively. It is, therefore, important to study the properties of SEI systemically to understand their influences on cell performance.

2.3 Characterization techniques

In this dissertation, multiple techniques were used to characterize electrochemical features, and chemical/physical and mechanical properties.

Electrochemical impedance spectroscopy, cyclic voltammetry and differentiate capacity-potential profiles were generally used to capture the electrochemical and kinetic features of the materials. X-ray photoelectron spectroscopy, time-of-flight secondary ion mass spectroscopy, Energy-dispersive X-ray spectroscopy were used to characterize the SEI's chemical properties. The films' physical properties were characterized by x-ray

diffraction/reflectivity, spectroscopic ellipsometry, nano-indentation, laser acoustic wave measurement were utilized to measure the mechanical properties. All the equipment and experimental details will be introduced in following chapters.

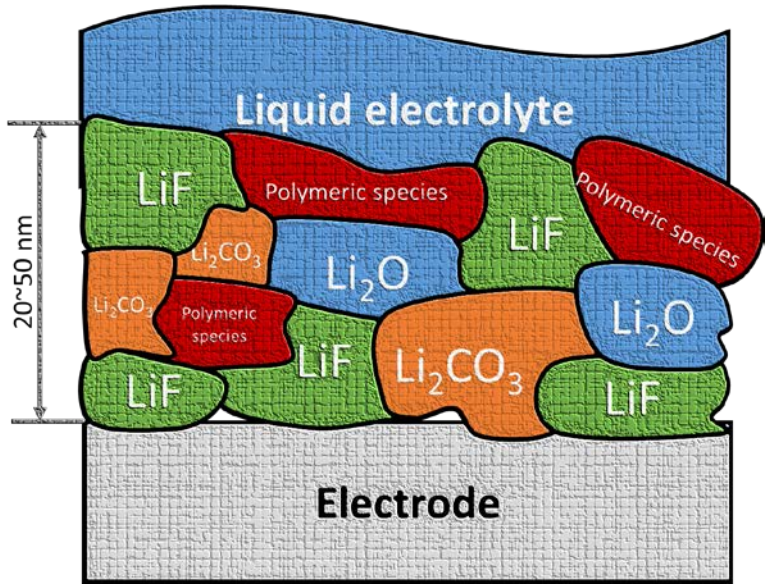

Figure 2.1 Schematic illustration of solid-electrolyte interphase

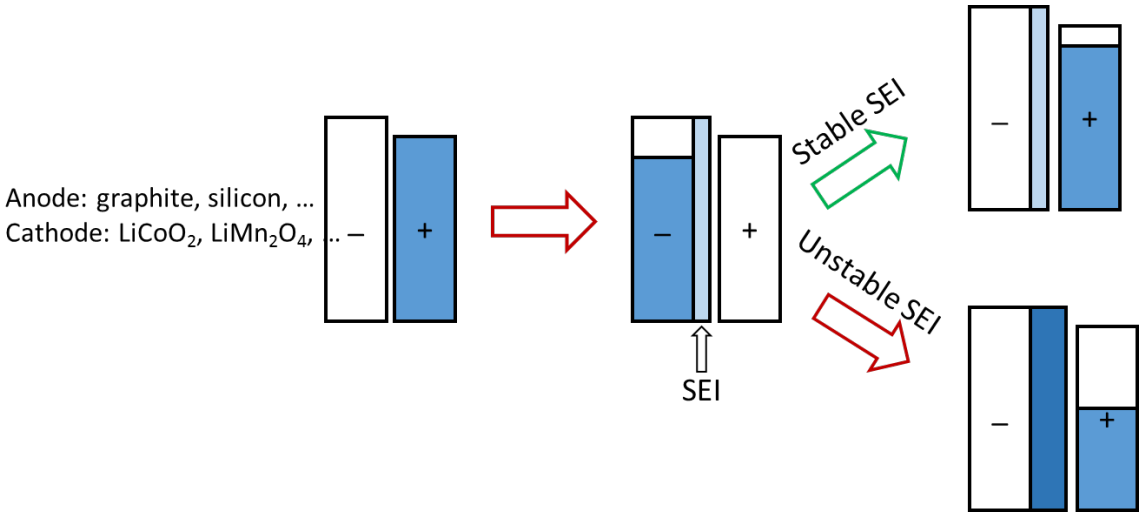

Figure 2.2 Schematic illustration of the available Li sources in the battery cell during cycling, with two cases: stable SEI and unstable SEI. The blue color indicates the amount of Li.

Chapter 3. The Study of Naturally Formed Solid Electrolyte Interphase: The Properties of Solid Electrolyte Interphase and Their Impact on Cycle Efficiency of Silicon-Based Negative Electrodes for Lithium Ion Batteries[1]

3.1 Summary

The solid electrolyte interphase (SEI) is a passivation layer formed on the electrode surface to ensure the long-term cyclability. An improved understanding of the relationships between the structure and properties of SEI is very important for revealing the capacity fading mechanisms, predicting the cycling stability, and designing high performance and durable electrode-coatings. In order to design better artificial SEI, we need to first understand the properties of SEI formed under natural electrolyte environment.

In this work, we were, for the first time, able to measure the mechanical properties of SEI formed on Si using a laser acoustic wave (LAW) method, and we correlated the SEI Young's modulus with its composition. Furthermore, we investigated the impact of mechanical and chemical properties of SEI over cycling and deduce the influence of SEI history on the Li-Si electrode behavior. We found that the inorganic components in the SEI led to higher elastic modulus and provided better mechanical protection as well as higher cycle efficiency. We envision this work can enable improvements in the design of artificial SEIs on electrodes that undergo large volume change, thereby leading to improvements in current efficiency and life of lithium ion batteries.

3.2 Introduction

There are growing demands for high energy and power density batteries, especially for electrical vehicle (EV) applications. Lithium ion batteries (LIBs) have been, among many energy storage systems, the choice for EVs. Many high energy density electrode materials have been studied for LIBs to meet the requirements for smaller weight and/or

[1] Reproduced from *Zhang, Q.; Xiao, X.; Zhou, W.; Cheng, Y.-T.; Verbrugge, M. W.; Toward High Cycle Efficiency of Silicon-Based Negative Electrodes by Designing the Solid Electrolyte Interphase Adv. Eng. Mater. 2015, 5, 1401398, DOI: 10.1002/aenm.201401398*

longer battery life. Silicon is able to deliver 3600 mAh g^{-1} by forming $Li_{15}Si_4$, which is 10 times higher than that of the graphite electrode used in commercial lithium ion batteries.[15-17] However, the huge volume expansion and contraction during the lithation and delithation processes lead to several critical issues, including material fracture and low cycle efficiency. Extensive efforts have been devoted to tailor the nanostructure, such as reducing Si particle size and developing Si based nanocomposites, to mitigate mechanical degradation. The low cycle efficiency, due to the unstable solid electrolyte interphase (SEI) on the Si electrode surface may become more critical, considering the significant increase in surface area when nano-scaled Si materials are used in negative electrodes. [18, 19]

The SEI is a passivation layer formed between the electrolyte (liquid) and electrode (solid). A stable SEI can effectively protect the electrode and prevent further decomposition of the electrolyte, thereby ensuring lithium ion battery cyclability with high efficiency. The stability of the SEI can significantly influence the Coulombic efficiency. For graphite and other electrode materials without large volume changes, the naturally formed SEI layer is stable and able to protect the electrode for thousands of charge-discharge cycles. However, for materials such as silicon, with a ~300% volume change during the charge and discharge, the desirable SEI must be able to accommodate the large volume expansion and contraction for stability. Recent research has shown that fracture is one of the main failure mechanisms of Si thin-film and/or Si particles.[20-22] Many approaches have been applied to stabilize the SEI on Si.[15, 23-27] Among them, both the ultra-thin coatings by atomic layer deposition and electrolyte additives showed promising improvements in the cycling performance of Si electrodes. [24, 25, 28] In order to design high performance and durable SEIs or engineer coatings as artificial SEIs, it is necessary to establish correlations between the structure, property, and performance of SEIs.

SEI's mechanical and chemical stability are crucial for the cycling life of electrode materials particularly with large volume change. In most cases, the SEI under investigation was formed on graphite. Previously, SEI layers have been characterized with a variety of techniques to identify the composition and chemical states.[29-31] SEI

contains organic and inorganic (crystalline) phases.[32, 33] The total resistance of the LIB cells can be obtained from electrochemical impedance spectroscopy (EIS). [34, 35] The formation of SEI can also be evaluated by EIS. The chemical stability of the SEI plays a dominate role for long-term cycle stability. Chemical composition can be characterized by X-ray photoelectron spectroscopy (XPS). Recently, more attention has been shifted to SEI formed on Si. [32, 36-39] However, measuring the mechanical properties of SEIs has been challenging because SEIs are only several nanometers in thickness, too thin even for nanoindentation measurements, which are commonly used method to measure the mechanical properties of thin films.[40]

In this work, we utilized several surface sensitive experimental techniques to characterize the elastic properties, chemical states, and electrochemical properties of SEIs prepared at different electrochemical potentials. We reveal the impact of mechanical properties of SEI on the electrochemical performance of a Si electrode. We believe that these results are useful for the design of coatings as artificial SEIs to improve the performance and cycle life of lithium ion batteries.

3.3 Experimental Section

Silicon thin-film electrodes with a thickness of 100 nm were deposited on copper current collectors by radio frequency (RF) magnetron sputtering system, and tested in coin cells for cycling stability. The Si electrodes were used as working electrodes, and pure lithium metal foil as counter and reference electrodes in CR2032 coin cells. A separator (Celgard, USA) was placed between working electrode and lithium foil, and 1M $LiPF_6$ in ethylene carbonate and dimethyl carbonate (EC:DMC 1:1 volume ratio, Novolyte USA) was employed for the electrolyte. The Arbin battery test system (BT-2000) was used to cycle the coin cells, using the constant-current method (with a rate of C/3) and a voltage window of 0.05 V to 1.5 V vs. Li. Before cycling, some of the coin cells were held at 0.5 V, 0.4 V, 0.3V, 0.2 V and 0.1 V for 100 hours. The EIS study was conducted in two-electrode coin cells at the assigned voltage. The coin cells were rested for 24 hours until they were stabilized. The high-frequency (Ohmic) resistance of the coin cells ranged from 400 to 500 Ohms. The applied frequency range for EIS measurements was between 1 MHz to 10 mHz.

Pouch cells were used for the formation of SEIs on Si wafers. N-type (100) direction Si wafers (Waferworld) were used in pouch cells. There are two reasons for using Si wafers: (1) single crystal silicon enables the best accuracy of LAW measurement and (2) Si wafers provide a similar surface environment to that of an actual Si electrode.[34] A piece of separator was placed between the lithium foil and wafer. At each side behind the wafer and lithium foil, there was a piece of copper current collector to connect to the electrical circuit (see Figure 3.1). The Bio-logic VMP3 potentiostat was used to hold the pouch cells to 0.4V, 0.2V and 0.05 V for 100 hours. (See Figure 3.2) After holding, the cells were charged to 1.2 V and held at 1.2 V until the current fell below 1 μA. This procedure ensures that the reversible Li is taken out, thereby reducing the samples' sensitivity to air. It is also difficult to define the interface between electrolyte and SEI. In our case, we cleaned the SEIs on silicon wafers with dimethyl carbonate (DMC), attached the wafers on sample stages with conductive tapes, and placed the sample stages in air-tight bottles for transfer. All these procedures were carried out in the glovebox to minimize the exposing time to air. The scanning electron microscope (SEM) images of SEI on Si wafer and cross-sectional SEM images were taken with an Hitachi S4800. The cross-sectional SEM samples were prepared by Hitachi IM4000 Cross Section & Flat Ion Milling system. Thermo Scientific K-Alpha XPS and PHI Quantera XPS Scanning Microprobe (Physical Electronics Chanhassen, MN) with a monochromated Al Kα source (1486.6 eV) were used for chemical analysis of SEI on Si. LAW equipment used for obtaining the mechanical properties of SEI was built by Fraunhofer Nanotech from Germany. The elastic properties were obtained by the fitting program of the LAW Analyzer.[41, 42]

3.4 Results and Discussion

The surface SEM images of Figure 3.3 show that SEI formed at 0.2 V (B) is much more uniform than that formed at 0.4 V (A). The surface morphology of SEI formed at 0.05 V (C) is rougher than others, which is because significant lithium was inserted into the top layer of the Si wafer.[43] The cross-section images of SEIs are shown in Figure 3.4.

From XPS depth profiles and spectra, Li, O, C, F, and a very low concentration of P can be found in all SEIs. The low P concentration at all depths indicates that a small number

of $LiPF_6$ salt molecules are trapped inside the SEIs (Figure 3.5).[44] All SEIs contain Li_2CO_3, LiO_2 and polymeric species. However, only SEIs formed below 0.4 V contain LiF. The majority of the F1s signal can be attributed to LiF. There is a greater amount of LiF in the SEI formed at 0.2 V than that formed under other potentials (See Figure 3.5, b, e and h). Using the spectra of F1s and Li1s along with depth profiles, we found the following concentration relation of LiF in the SEIs formed under the three potentials:

$$\text{LiF: } 0.2\,V > 0.05\,V > 0.4\,V$$

The C1s and L1s spectra provide information about Li_2CO_3 and Li_2O. The SEI formed at 0.4 V contained mostly Li_2CO_3 and Li_2O. The formation of Li_2O can be attributed to the instability of Li_2CO_3 ($Li_2CO_3 \rightarrow Li_2O + CO_2$), since Li_2CO_3 can be decomposed by Ar^+ sputtering.[45] But Li_2O is also found before sputtering (see Figure 3.7). The overall Li concentration is about the same for all samples (Figure 3.6), the ratio of different Li species can be obtained from the peak areas in Figure 3.5 g, h and i. The SEI formed at 0.2 V contains the least amount of Li_2CO_3 (see C1s spectrum Figure 3.5e), and Li_2CO_3 is more concentrated near the surface (see Figure 3.9). The overall concentration relation of Li_2CO_3 in SEIs can be represented as:

$$Li_2CO_3 \text{ and } Li_2O\text{: } 0.4\,V > 0.05\,V > 0.2\,V$$

The Si thin films were prepared on rough Cu surface). The atomic percentage of Si after sputtering for a certain time is another indicator of the SEI film thickness, as less Si implies a thicker SEI film. Accordingly, the thickness of SEI formed at 0.4 V is greater than 0.2 V and 0.05 V (Figure 3.6). This is consistent with the SEM observations.

Figure 3.10 shows the Nyquist plots of EIS spectra for the different voltages. The semicircular regions of the Nyquist plots are usually related to interfacial impedance, including that of the SEI and charge-transfer reactions. The first semicircle at high frequency corresponds to the surface passivation layer, the SEI, and the second semicircle corresponds to the charge transfer reaction. [46] At the low frequency region, the sloping line corresponds to diffusion resistance (ideally, the Warburg resistance). During the 100 hours of SEI formation at 0.4 V, the electrolyte decomposition is incomplete, and the SEI composition is neither uniform nor stable. When the electrode is held at a lower voltage,

such as 0.05 V, there is additional SEI formed. During the 100 hours of SEI formation at 0.2 V, the current drops to a very low value, indicating a near-equilibrium condition and cessation of electrolyte decomposition. Hence, the SEI film is a stable and a uniform passivation layer has been formed over the surface of electrode, which can provide protection to the electrode. After discharge of the electrode to 0.05 V, there is no measureable increase in resistance. Compared with the electrode held at 0.05 V for 100 hours, the overall resistance of electrode held at 0.2 V is smaller as well (cf. Table 3-2 and Figure 3.10 Nyquist plots of AC impedance spectra of Si electrodes with different SEI films; left: 3D plots of EIS measurements under each holding voltages and 0.05 V; right: 2D plots of EIS measurements under 0.05 V only.). The overall resistance of the cells under the 0.05 V operating voltage is:

$$\text{Impedance: } 0.4\,V > 0.05\,V > 0.2\,V$$

Young's modulus is very sensitive to the structure of material. The velocity C of surface acoustic wave (SAW) is related to Young's modulus E, Poisson's ratio v and density ρ.

$$C = \frac{0.87 + 1.12v}{1 + v}\sqrt{\frac{E}{2\rho(1+v)}}$$

There is a property of SAW, the depth of SAW is proportional to the wave length: the higher the frequency, the smaller the depth penetration of the SAW. As a result, the phase velocity (SAW velocity v) depends on frequency$f$, and the relation between v and f called dispersion. The phase velocity is defined as:

$c = c(E, E', v, v', \rho, \rho', d, f_k)$

E: modulus of substrate, E' : modulus of film

v: Poisson$'$s ratio of substrate, v' : Poisson$'$s ratio of film

ρ: density of substrate, ρ' : density of film

d: film thickness

f_k: frequency along k direction

The density of the SEI film is calculated by the ratio of possible components. From XPS analysis, we assumed that LiF contributed to the F1s signal and Li_2CO_3 contributed to C1s signal. The Poisson's ratio was assumed to be 0.22. Thickness was measured by cross-sectional SEM.

The procedure of commercial fitting program LAW Analyzer is based on the principle of minimizing the least-square errors:

$$Min\left\{\sum_k [c(f_k) - c(E, E', v, v', \rho, \rho', d, f_k)]^2\right\}$$

$c(f_k)$ indicates the measured curve and $c(E, E', v, v', \rho, \rho', d, f_k)$ is the theory curve. Details about this part are described in reference [47-50]

The LAW method is used to measure the Young's modulus of the SEIs. The SEIs were electrochemically formed on Si wafers in a pouch cell. (Details on making the pouch cells can be found in 3.3 Experimental Section.) Before testing the mechanical properties of the SEIs, a silicon wafer was tested by LAW system to obtain the mechanical properties of the substrate. The blue line in Figure 3.11 is the dispersion curve of the Si substrate along the [110] direction (primary flat). The phase velocity is 5081.32 ± 0.30 m s^{-1} with the variation smaller than 0.6 m s^{-1}, which indicates that the wafer is clean and the LAW system is working properly. The phase velocity refers to the theoretical velocity of (100) wafer along the [110] direction.[50] A few monolayers of silicon oxide can cause a small decrease in the phase velocity with increasing frequency. The fitting results for the substrate are shown in Table 3-1. The elastic properties determined for the Si wafer agree well with published values.[40] (Details about LAW methods and theories are described in Supporting Information and references.[41, 42, 51, 52]) The values in Table 3-1 were also used to obtain the moduli of SEI films.

The blue, red and green solid lines are dispersion spectra of different SEI films formed under 0.2, 0.4, and 0.05 V, respectively. In order to fit the dispersion curves to obtain Young's modulus values, the thickness and density need to be obtained by other independent techniques. Specifically, the thickness of the SEI film is measured from

cross-section SEM. (see Figure 3.4). The blue and red dots are the fitting results based on minimizing the least-square error for SEI formed at 0.2 V and 0.4 V. The other important parameters and Young's moduli are shown in Table 1. Both fitting results of 0.2 and 0.4 V samples show reasonable moduli of substrates. The substrates' moduli match well with the C11 theoretical modulus of single crystal silicon.[40] The Young's modulus of SEI formed at 0.05 V cannot be obtained, because of its high interfacial roughness (Figure 3.3). The voltage of 50 mV is below the voltage where amorphization of Si by lithiation occurs, causing the change of substrate properties. [43] As it is shown in Table 3-1, the Young's modulus of SEI formed at 0.2 V is 69.2 GPa, larger than SEI formed at 0.4 V, 42.1 GPa. From cross-section SEM images, we found that SEI formed at 0.2 V is thinner than that of 0.4 V.

Coulombic efficiency is an important indicator to evaluate the cycling stability of electrodes. Si thin films with SEIs formed under a controlled potential holding have been tested in coin cells (see Experiments section). Figure 3.12 (a) shows that the controlled SEI formation process at various fixed voltages leads to significantly improved Coulombic efficiency (red and blue dots) when compared with the control sample (black). After the cycle stabilized (after 10 cycles), the samples held at 0.2 V shows the best Coulombic efficiency, 99.87±0.03%. Figure 3.12 (b) shows that the average Coulombic efficiency of the first 100 cycles for various initial holding potentials, ranging from 0.5 V to 0.1 V. We find that 0.2 V is the optimal holding potential to achieve the best cycling performance.

Naturally formed SEIs usually contain inorganic species (such as LiF and Li_2CO_3) and organic polymers.[53] The less dense organic species are usually contained in thicker layers than the inorganic species. The inorganic components also introduced greater resistance of the surface films due to the poor ionic conductivity. In our case, the SEI formed under 0.4V contains the most inorganic species, hence greatest resistance. The stability of inorganic salts is also better than the organic species (in this work, we do not consider organic additives used to stabilize the surface). LiF has been widely believed to lead to protective films over the surface of Si electrodes, and LiF has been associated with improved cycling stability, especially when fluoroethylene carbonate (FEC) is

employed as an electrolyte additive.[36, 37, 39] Previous research has shown that LiF contributes to the improvements of cycling stability, perhaps because LiF is unlikely to be dissolved in organic electrolytes.[25, 36, 37, 54] The good cycling performance of the 0.2 V prepared SEI (Figure 3.5) is thus likely caused by its high concentration of LiF. Thus it would appear that relation between performance (in terms of Coulombic efficiency) and surface chemistry can be exploited. Samples with a higher concentration of LiF on surface show higher Coulombic efficiency; however, higher concentrations of Li_2CO_3 show lower Coulombic efficiency. This work shows that, by certain potential treatment, favorable species in terms of a robust and protective SEI can be increased, thereby improving the cycling performance.

The elastic properties of SEIs formed on the surface can influence the cycling performance. One major issue with Si based electrodes is the cracks generated during charge-discharge cycles. In accommodating the large volume change, cracks may be generated to release built-up strain energy. Additional SEI forms on crack-generated new surfaces. Furthermore, cracks can isolate the electrode material, losing electrical contact and capacity permanently. This coupled mechanical and chemical degradation can be reduced by surface engineering, including surface coatings and controlled SEI formation.[28] In our study, thin-film Si electrodes were used during the test. The majority of volume expansion is along the thickness direction. SEI formed under 0.2 V is stiffer than that of 0.4 V (higher Young's modulus). Stiffer films attached to the Si surface will increase the energy barrier for crack nucleation and propagation, and reduce the formation of micro-cracks on Si electrode surfaces. Stiffer SEI films can also help reduce micro-crack formation significantly, leading to improve cycling stability.

3.5 Conclusion

In summary, SEI films formed under different potentials have been characterized including electrochemical behavior, surface chemistry, and, for the first time, mechanical properties. We reveal the relation between the cycling efficiency and properties of the SEIs. Stiffer SEIs provide better protection for Si thin film electrodes due to the increase in the energy barrier for crack formation and propagation; low resistance and LiF rich are favorable for improving the cycling efficiency. This work provides an improved

understanding of the relation between SEI properties and cycle performance, thereby enabling improvements in the design of artificial SEI on electrodes that undergo large volume changes.

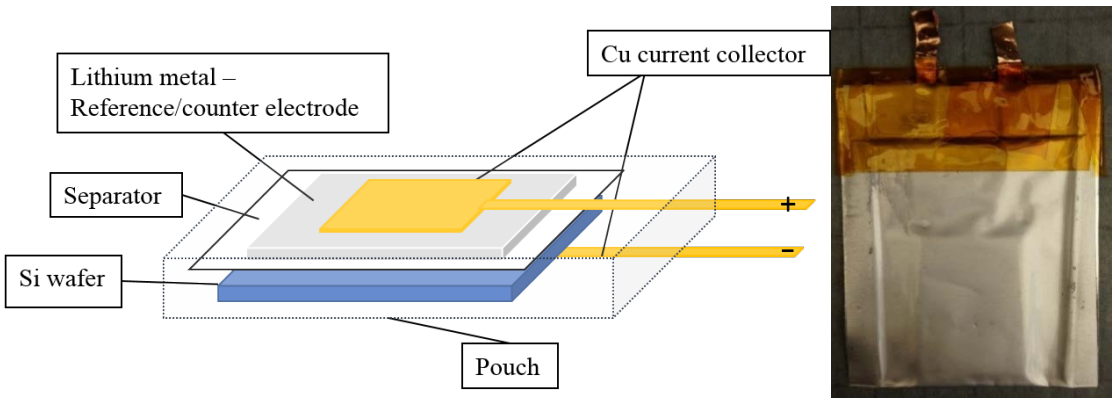

Figure 3.1 Schematic figure of the setup of pouch cells (left); photo of single layer pouch cell (right)

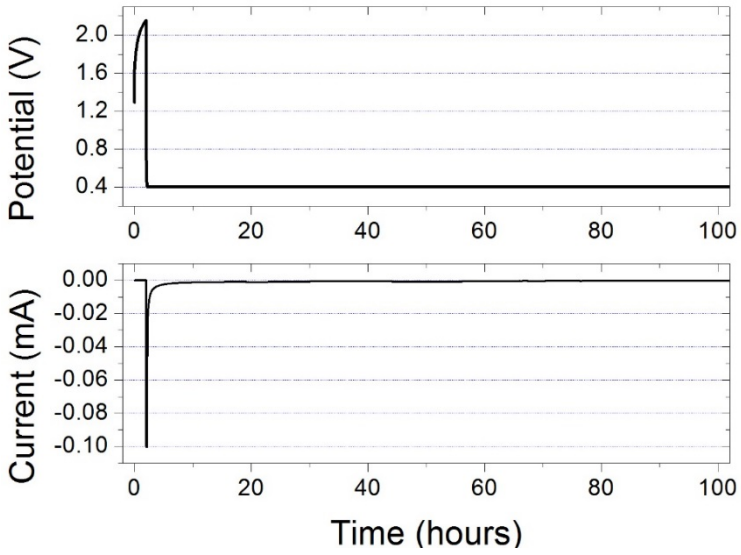

Figure 3.2 Potential holding process example: 0.4 V. Top: potential profile v.s. Li/Li+; bottom: current response.

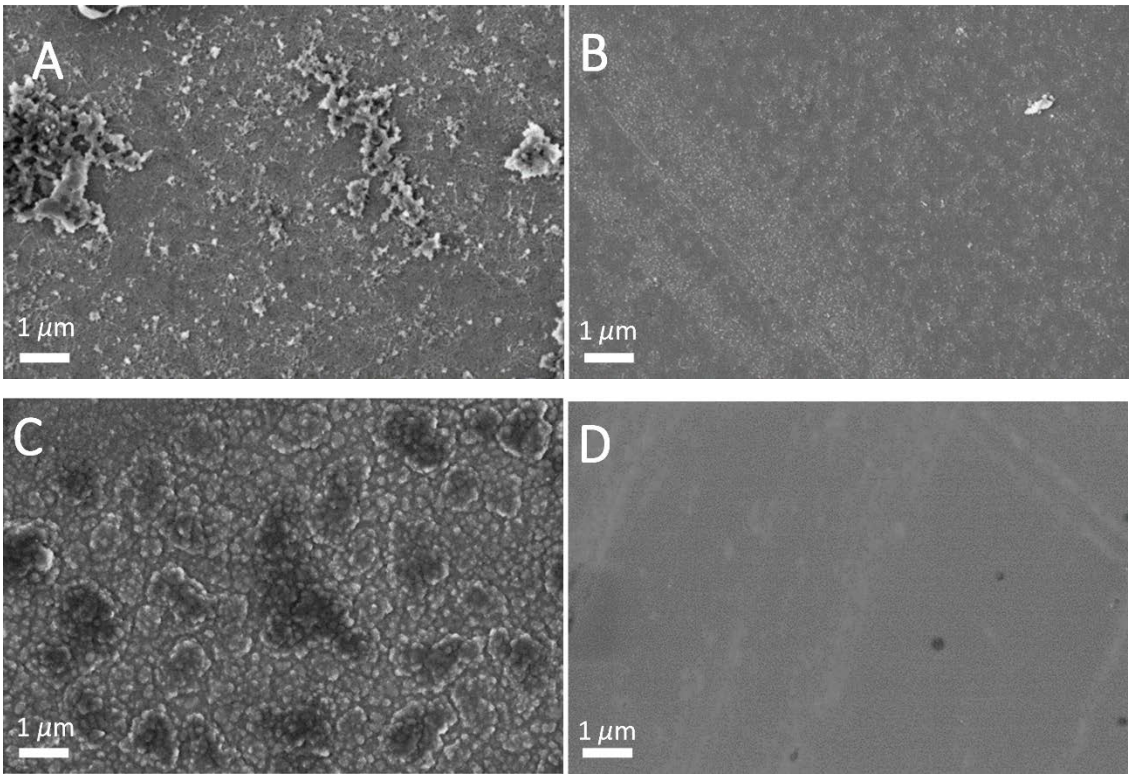

Figure 3.3 SEM images show the surface morphologies for different SEI formations. A: 0.4 V; B: 0.2 V; C: 0.05 V and D: bare silicon wafer

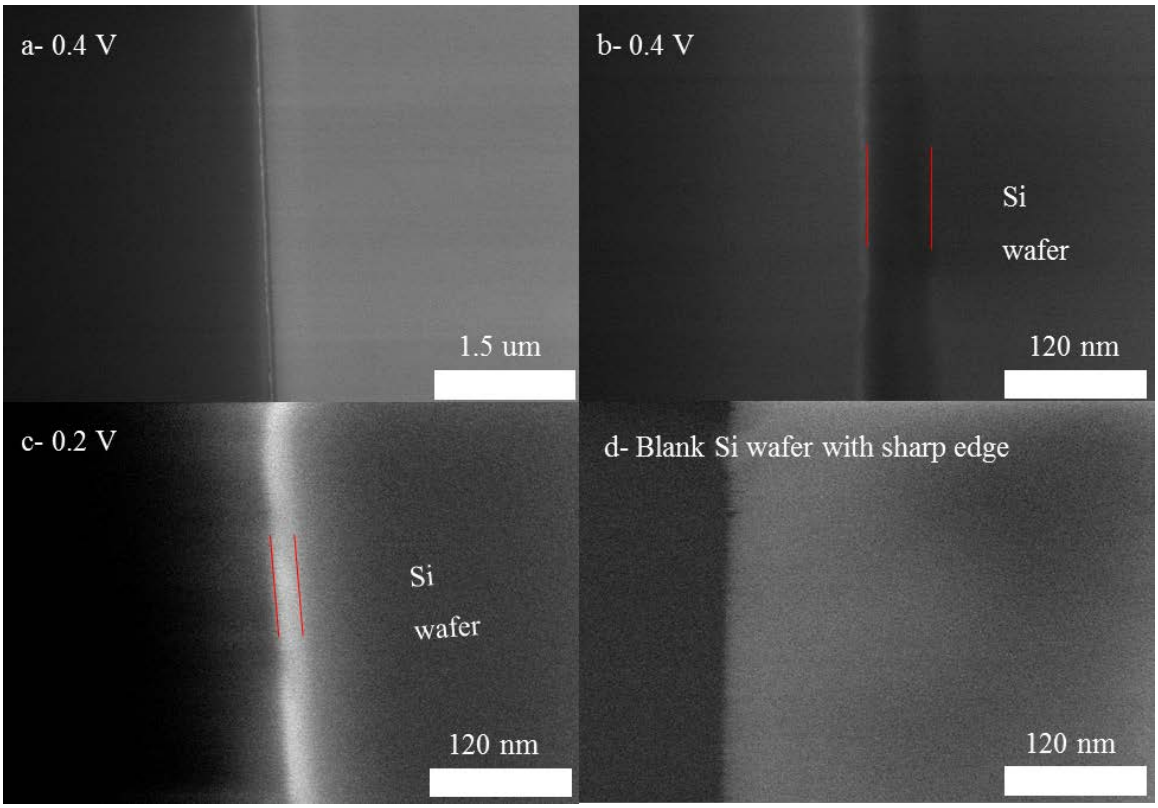

Figure 3.4 Cross-section SEM image of SEI sample hold at 0.4 V/0.2 V. The thickness of SEI hold at 0.4 V is about 57.18 nm (a and b), the thickness of SEI hold at 0.2 V is about 24.31 nm (c). The lower right corner image shows the sharp edge of blank silicon wafer, as a comparison group (d).

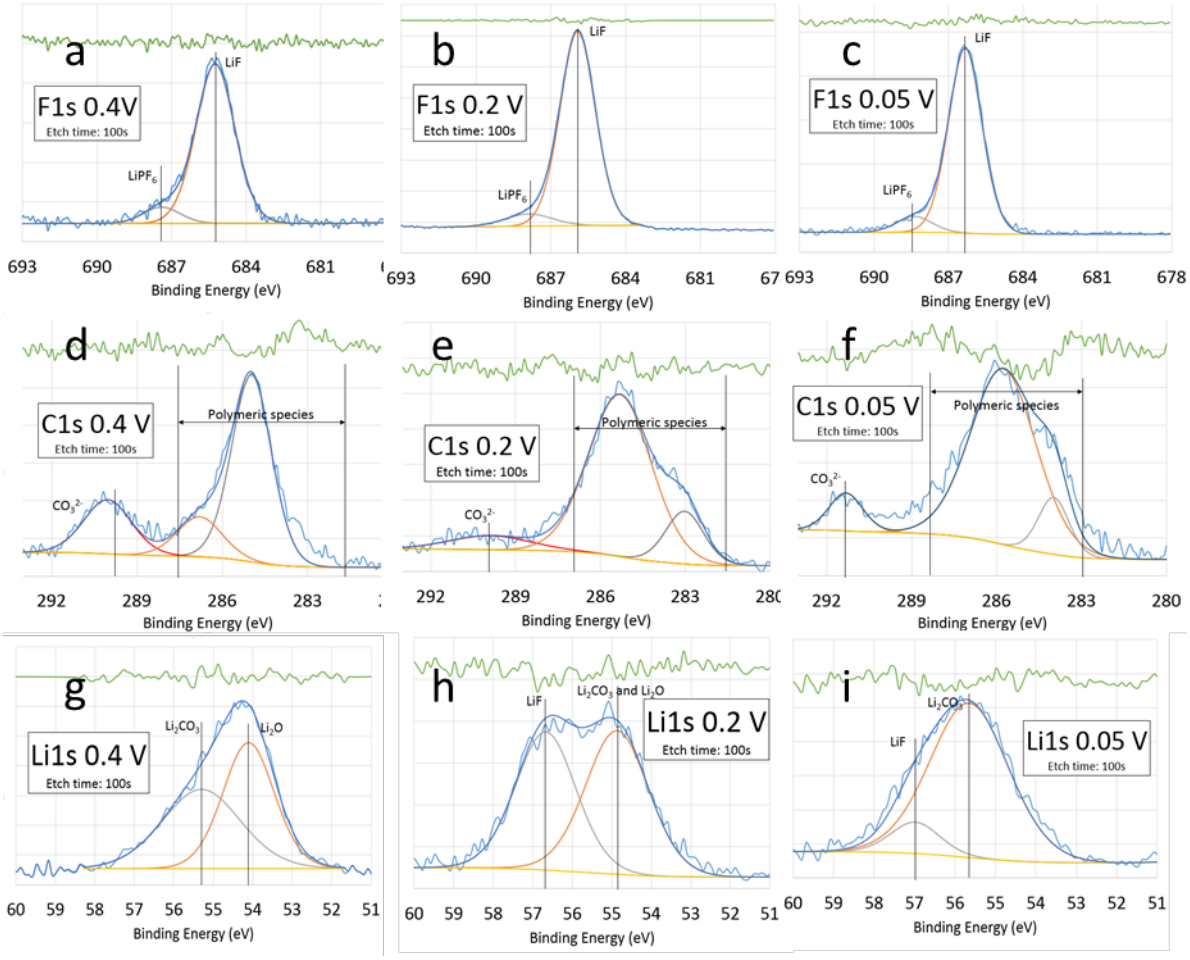

Figure 3.5 XPS F1s, C1s and Li1s spectra of silicon electrode sample with 0.4 V, 0.2 V and 0.05 V potential treatment for 100 hours.

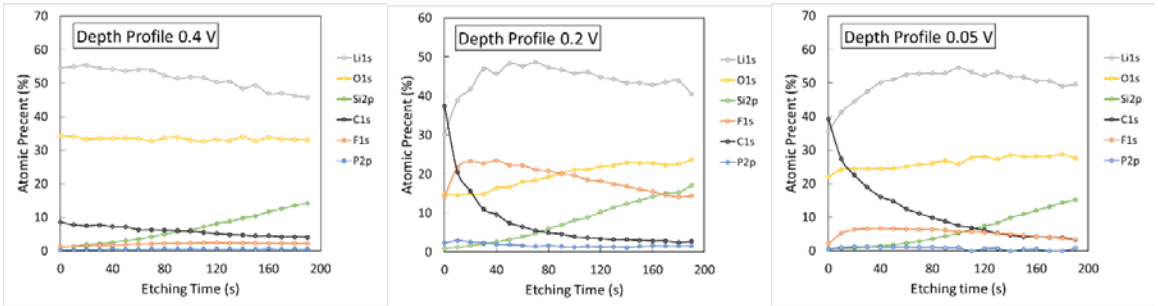

Figure 3.6 XPS depth profile of Si electrode with 0.4 V, 0.2 V and 0.05 V potential treatment

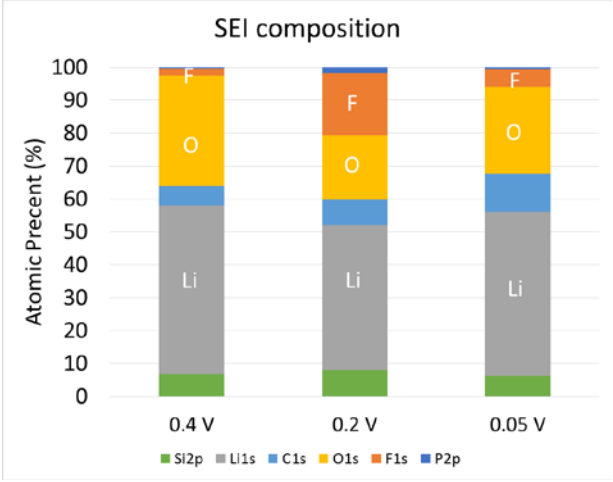

Figure 3.7 Average concentration of different SEIs for etching time of 200s.

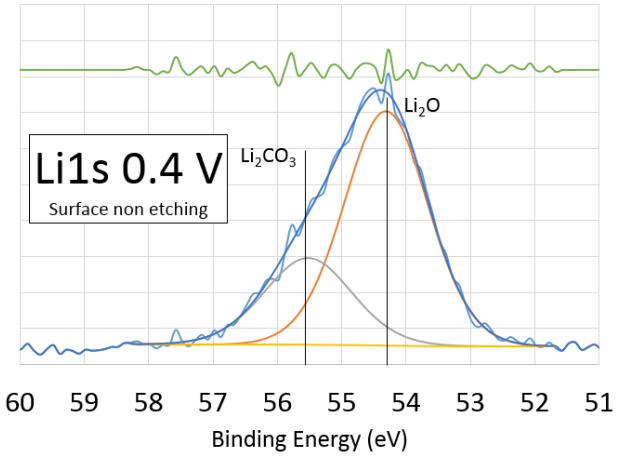

Figure 3.8 XPS Li1s spectrum of SEI film formed at 0.4 V without etching (surface)

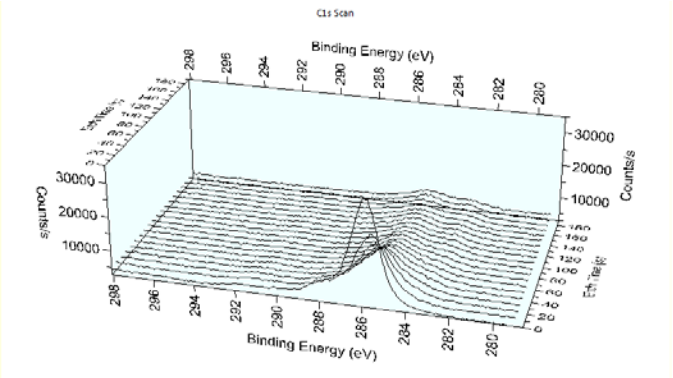

Figure 3.9 C1s spectra-depth profile of SEI film formed at 0.2 V.

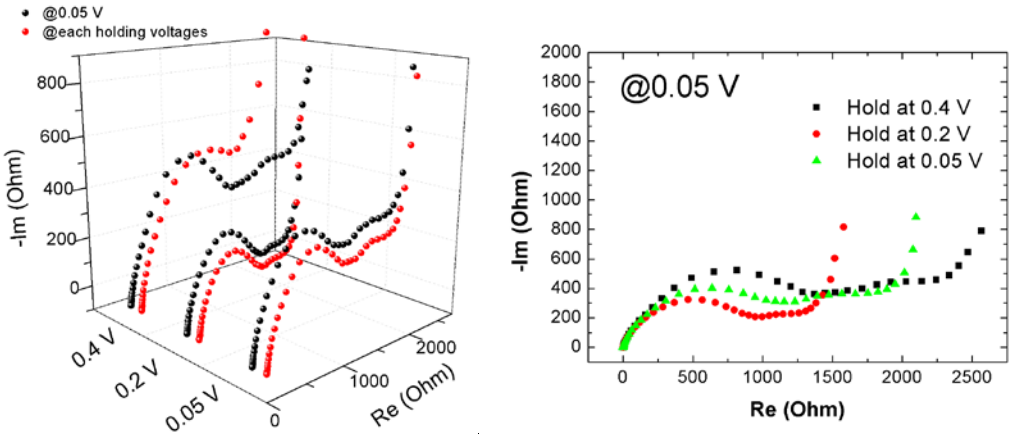

Figure 3.10 Nyquist plots of AC impedance spectra of Si electrodes with different SEI films; left: 3D plots of EIS measurements under each holding voltages and 0.05 V; right: 2D plots of EIS measurements under 0.05 V only.

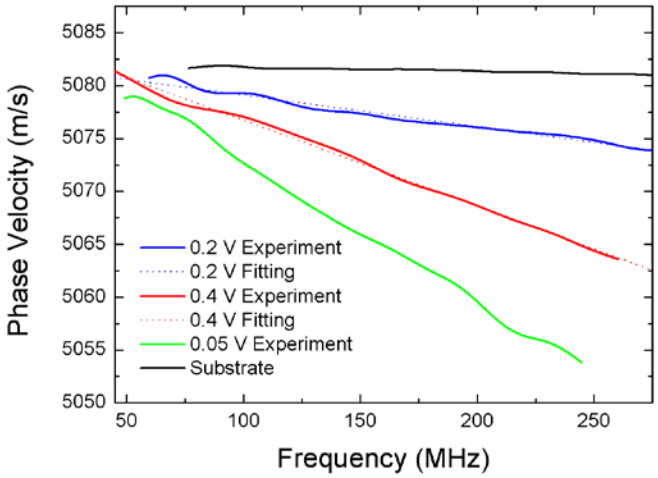

Figure 3.11 Dispersion curves obtained from LAW measurement and fits for 0.2 V and 0.4 V holds.

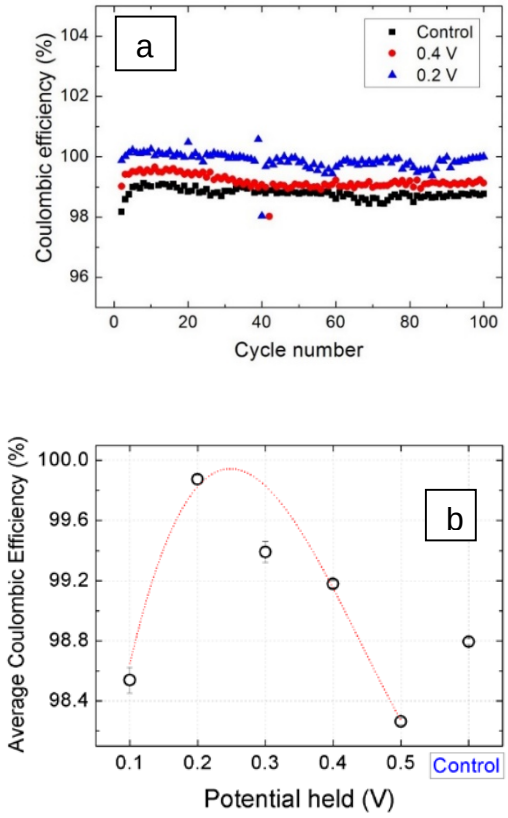

Figure 3.12 (a) Comparison with Coulombic efficiency of samples with different potential holds of 100 hours. Blue: 0.2 V, red: 0.4 V, black: controlled experiment without holding; (b) average Coulombic efficiencies of first 100 cycles for potentials holds ranging from 0.1 to 0.5 V with standard error bars. (The error bars for 0.2, 0.4 and 0.5 V overlapped with the dots) The red dot line shows just the trend line.

Table 3-1 Young's modulus obtained from [110] direction of N-type (100) silicon wafer by LAW measurements

	C11	C12	C44
Young's modulus (GPa)	165.568 ± 0.077	63.520 ± 0.127	79.527 ± 0.022

Table 3-2 Summary the properties of different SEI films

Preparation method	**Under 0.4 V for 100 hours**	**Under 0.2 V for 100 hours**
Average Coulombic efficiency (%)	99.18 ± 0.02	99.87 ± 0.03
Thickness (nm)	57.18 ± 0.18	24.31 ± 0.15
Young's modulus (GPa)	48.08 ± 1.29	69.18 ± 2.40
Resistance* after 100 hours (Ohm)	1276.93 ± 11.92	1204.76 ± 16.94
Resistance* at 0.05 V (Ohm)	2301.18 ± 12.22	1354.84 ± 8.89
Uniformity	Rough	Uniform
Chemical composition	Li_2CO_3 (+ Li_2O) + Polymeric species	LiF+Li_2CO_3 (+ Li_2O) + Polymeric species

*Resistance is defined by the semicircles

Chapter 4. A Non-Destructive Method to Measure the Mechanical Properties of Artificial Solid Electrolyte Interphase[2]

4.1. Summary

The mechanical properties of ultrathin, protective films are critical for the reliability of Li-Si negative electrodes; however, it has been a challenge to get reliable measurements of the critical mechanical properties for further optimizing the system due to the influence from the substrate. In this work, we used a non-destructive method - laser acoustic wave measurement - to study the elastic properties of protective Al_2O_3 thin films. Al_2O_3 is widely used as artificial SEI on lithium-ion battery electrodes. The measured properties were consistent with previous work using other complicated and destructive approaches, such as nanoindentation. This straightforward approach can be easily applied to measure the mechanical properties of various ultrathin films for multiple applications, including the mechanical properties of the (artificial) solid electrolyte interphases (SEIs), and thus enables methods to improve the cycle and calendar life of lithium ion batteries.

4.2. Introduction

Atomic layer deposition (ALD) is a thin film preparation technique which the film is grown layer-by-layer. Since it is a self-limiting surface reaction process which involves alternatively inputting different precursor for one cycle, the thickness of ALD coating, and can be precisely controlled by the cycle number. [55, 56] Also, the gaseous precursors can contact with any substrate surfaces exposable to gas, so thin films can be deposited on, for the most part, any shape and geometry.[55, 57] ALD can be used to deposit oxides (Al_2O_3, HfO_2, TiO_2, ZnO, etc.),[58-61] sulfides (ZnS, SrS, etc.),[62, 63] fluorides (CaF_2, LaF_3, etc.),[64, 65] metals (Ir, Pt, etc.)[66, 67] and polymers (PMDA, etc.)[68]; the nature of the coatings strongly depends on the precursors selected. ALD has been widely used in various applications, for instance, high-*k* gate oxides,[69, 70]

[2] Reproduced from *Zhang, Q.; Xiao, X.; Cheng, Y.-T.; Verbrugge, M. W.; Appl. Phys. Lett. 2014, 105, 061901*

passivation of crystal silicon solar cell,[71, 72] coating of nanoporous structures,[63, 73] metal coatings for fuel cell catalyst layer,[74, 75] adhesion layers.[76] The rapid development towards scaling down device size, improving performance, functionality, and reliability by the microelectronics industry has been enhanced by nanotechnology, particularly by ALD. Very recently, ALD has been employed for surface modification of different components in lithium ion batteries (LIBs), including negative and positive electrodes and separators, to mitigate the undesirable side reactions and improve the battery life.[77-80]

In those applications, the mechanical properties of the ultrathin thin films are the key. The mechanical properties for low dimensional materials, such as ALD films, are typically different from the material's bulk properties, primarily because of the differences of materials structures, and the large ratio of surface area to volume. The mechanical properties are critical for high-*k* dielectrics. The elastomechanical response to thermal cycling will significantly influence the compatibility and long term reliability. An objective for the use ALD coatings on lithium ion battery electrodes is to suppress electrolyte reduction as well as to stabilize the inherent SEI layers that form during cell operation, thereby suppressing mechanical fracture in the electrodes, which can be problematic for high lithium-capacity materials, such as Si and Sn. Understanding the elastic properties of thin films will be indispensable for designing the electrode coatings for high energy electrode materials with huge volume change (over 300%) and internal stress during lithiation and delithiation.[28]

Nanoindentation (NI) has been applied to obtain the Young's modulus of ALD thin films.[81] NI tests require the depth of indents less than 1/10 of the film thickness to neglect the influence of the substrate. For such studies, the ALD films need to be thick, such as 300 nm. The effective deposition rate (thickness increment per time unit) of ALD is low. Films of 300 nm require approximately 2000 reaction cycles, which can lead to time-consuming processing. Other testing methods, such as bulge testing and pointers,[82] require either thick films or complicated substrates.

In this work, elastic properties of ALD alumina thin coatings were characterized by laser acoustic wave (LAW) method. LAW is a non-destructive sonic technique to obtain the

mechanical properties of thin films. It has been successfully applied to coatings such as diamond like carbon (DLC), silicon nitride, etc.[50, 83] The LAW technique, along with other characterization methods, enabled us to obtain the elastic properties of thin ALD films in a straightforward manner. At the same time, we also measured the influence of deposition temperature on elastic properties of ALD Alumina films.

4.3. Experimental Section

Al_2O_3 thin coatings were grown on (100) Si wafer (etched with 10% HF water solution to reduce the influence of native SiO_x surface species). Trimethylaluminium (TMA) and high performance liquid chromatography (HPLC) water were used as precursors in the ALD system. The pulse time is 0.015 s, exposure time is 2 s, and purging time is 8 s for both precursors. The growth temperature is chosen as 120 ^oC for LIB applications. Higher temperatures lead to the damage of polymer binders in the electrode, and lower temperatures lead to poor film quality. The thickness of Al_2O_3 films were controlled by cycle numbers, ranging from 50 to 250 cycles.

For measuring the influence of deposition temperature on ALD films' elastic properties, deposited 150 of ALD reaction cycles under different temperatures, ranged from 60 ^oC to 160 ^oC.

Young's modulus is very sensitive to the structure of material. The velocity (c) of surface acoustic wave (SAW) is related to Young's modulus E, Poisson's ratio v and density ρ:

$$c = \frac{0.87 + 1.12v}{1+v}\sqrt{\frac{E}{2\rho(1+v)}}$$

By generating different frequencies of sound waves, the modulus can be fitted with the predetermined density, thickness, and Poisson's ratio. The depth of the SAW is proportional to the wave length, for example, higher frequencies lead to smaller penetration depths by the acoustic waves. The phase velocity is frequency dependent and is influenced by the substrate and the film; however, the film contribution dominates at higher frequencies. The relation between frequency and phase velocity (called dispersion relation) can be obtained for the set up, and thereby used to determine the mechanical properties of thin films. Experiments provide us the dispersion curve, the relation

between phase velocity and frequency, and the aforementioned model can be used to fit the experimentally obtained dispersion curves by the least squares method. Details can be found in references.[47-50] In order to obtain the right elastic properties of thin films using LAW, thickness and density needs to be measured with other techniques independently as the inputs for LAW Analyzer. LAW equipment (Fraunhofer Nanotech) was used for obtaining the dispersion curves. The measuring distance was 10 cm.

X-ray reflectivity (XRR) techniques use X-ray reflection intensity curve from a grazing incident beam to determine the thickness and density of thin films. XRR was performed with a Bruker D8 Advanced, with 2 theta varying from 0^o to 8^o. The X-ray wavelength from Cu $K\alpha$ was 1.54 Å. The voltage and electron beam current were controlled at 40 kV and 20 mA, respectively. Thickness and density were then obtained by fitting the XRR data (Bruker Leptos). In addition, ellipsometry measures the thickness by the change in polarization state of light reflected from the surface of a sample. Electron probe microanalysis (EPMA) was used to verify the density of ALD films. Data were collected in static and in scanning mode over a 30 μm area at 10 different positions in the sample. The electron beam conditions were 20 kV and 20 nA. The Si, Al, and O x-ray intensities from the samples and standards (pure Al, pure Si, and $SrTiO_3$) were used to estimate the area density of the Al_2O_3 coating on the Si substrate using thin film modeling program GMRFILM. LAW equipment (Fraunhofer Nanotech) was used for obtaining the dispersion curves.

4.4. Results and Discussion

4.4.1. Thickness and density of films

Figure 4.1 shows the thickness and density of all films with 50 to 250 reaction cycles. The blue dots show the thicknesses of ALD alumina films ranging from 7.6 nm to 37.9 nm by XRR, corresponding to 50 to 250 reaction cycles. The average growth rate is 1.5 Å/cycle. The linear relation is shown as the dashed line. By fitting the XRR data, the thickness and density are estimated simultaneously. The density ranges from 3.1 to 3.4 g/cm^3, with an average density of 3.26 g/cm^3 (triangles in Figure 1). EPMA is also used

to estimate the density for sample with 250 reaction cycles. The area density obtained is 11.8 ± 0.2 μg/cm^2. By inputting the thickness information obtained from XRR (37.9 nm), we are able to estimate the density of the film. The density extracted by EPMA is 3.11 g/cm^3, which matches well with the XRR results (Table I). Both thickness (growth rate) and density match well with previous ALD work.[84] EPMA also provides the composition information about the sample. The sample contains 44.8 % of Al and 55.2 % of O in terms of atomic percent. The low concentration of O is consistent with oxygen deficiency. Previous studies show that the O vacancies in ALD amorphous films have similar parameters in crystalline α-Al_2O_3 and γ-Al_2O_3. [85]

4.4.2. Elastic properties of alumina ALD films

SAWs propagate parallel to the surface measured, and they interact significantly with the film on surface, with penetration depths as thin as 1/100 of the wavelength.[47] Hence, SAWs are suitable for determining the elastic properties of very thin films. In our experiments, the use of single crystal silicon substrate enables us to obtain the phase velocity accurately for ultra-thin films. (*thickness* < 20 nm) Other polycrystalline substrates, such as steel, can cause ultrasonic scattering and reduce the sensitivity of the measurements.[41]

Figure 4.2 shows the dispersion relation (phase velocity versus frequency) for all films. The number on up-right corner of each figure is the reaction cycle number. As would be expected, for the pure silicon substrate, the phase velocity of SAW doesn't change significantly with frequency range of 50 to 230 MHz. All the diagrams in Figure 2 show that the alumina films decrease the phase velocity with increasing frequency. The phase velocity descends faster with increasing the alumina thickness. As described previously, the phase velocity is dependent on elastic properties, density of both substrate and film, and the thickness of the film; and the film thickness and density can be determined by XRR and EPMA. The elastic properties of substrate are provided in Table 3-1. The values agree well with published values. The density of Si substrate is 2.33 g/cm^3. Poisson's ratio of Si is 0.22, alumina is 0.21. With these parameters, we are able to obtain the Young's modulus of the films by fitting the model (dashed line) to the experiment data (solid line). The Young's modulus is shown in Figure 4.3 and Table 4-1. The

thinnest film, with 50 reaction cycles (7.6 nm thick), shows slightly lower Young's modulus. The others modulus values range between 170 and 180 GPa: there is no significant change of Young's modulus with increasing the thickness of film. The last row of Table 3-1 shows the extracted modulus for the substrate. The values are close to measured and theoretical values for single-crystal Si.

According to our measurement of alumina ALD films ranging from 7.6 to 37.9 nm, there is no obvious trends for of elastic properties, density, or growth rate varying with thickness, which indicates that the structure of the ALD films is substantial invariant. The thickness range we measured cannot be used to revel the material properties at the Si-alumina interface, as the interfacial transition layer is only a few atomic layers (usually less than 5 Å), and the thinnest ALD film we can measure is about 80 Å. We expect the interfacial zone is less than 10% of the total measured film thickness. To date, we are not aware of an experimental technique that enable one to extract elastic properties for film less than 1 nm in thickness; hence, computational modeling is helpful in terms of understanding the ALD interfacial effects.

The Young's modulus values obtained from this work is comparable with literature values. Higher ALD deposition temperatures will produce stiffer films (cf. Table 4-3). As mentioned, nanoindentation usually requires film thicker than 100 nm as the indent depth should within 1/10 of the film thickness to neglect the influence of substrate. If nanoindentation is used to obtain Young's modulus for films thinner than 100 nanometers, both continuous stiffness measurement and modeling are necessary. The nanobeam deflection method requires a complicate sample fabrication. The films we measured using LAW method, thickness ranging from 7.8 nm (50 reaction cycles) to 38 nm (250 reaction cycles), are much thinner than prior work. The measurement is simple and fast, as well as non-destructive. This method can be applied to most ALD films to obtain the elastic properties.

The density of ALD alumina films (~3.2 g/cm3) is lower than reported crystal density (3.9 - 4.1 g/cm3) and amorphous density (3.5 - 3.7 g/cm3) for Al_2O_3,[86] due to the low deposition temperature. This agrees with the previous study of ALD. [84] The EPMA results show a relative low concentration of oxygen atoms, indicating the oxygen

deficiency. That leads to the lower modulus values, 170 - 180 GPa, as compared to single crystal Al_2O_3 (530 GPa)[87] and many ceramics (344.83 - 408.99 GPa. [86]). However, lower modulus is favorable in many cases. For example, low modulus coatings can usually better accommodate the volume change of the substrate material, particularly for Si based high capacity electrode materials in lithium ion batteries.

4.4.3. Influence of ALD deposition temperature on elastic properties

Figure 4.4 shows the dispersion curves for alumina ALD samples deposited under different temperature, which are similar with Figure 4.2. The deposition temperature is shown in the upper-right corner of each figure. By using XRR to measure the thickness and density of the films, we can obtain the elastic modulus of each film. Figure 4.5 shows the elastic properties of the films deposited under different ALD deposition temperature. The general trend is, higher temperature leads to higher density of the film, hence larger values of elastic moduli. Table 4-4 shows the detail properties of ALD films deposited under different temperature.

4.5. Conclusion

In this work, we develop and implement a non-destructive method to obtain the mechanical properties of ultra-thin ALD (atomic layer deposition) films. The mechanical properties are critical for designing coatings for many applications. We used ALD alumina coatings to demonstrate the approach, as such coatings are of immediate interest for lithium ion batteries. With the LAW (laser acoustic wave) technique, along with XRR (X-ray reflectivity), we are able to extract the mechanical properties of ALD films as thin as a few nanometers. The Young's modulus was found to be relatively constant for thicknesses ranging from 7.6 to 37.9 nm, corresponding to 50 to 250 reaction cycles, respectively. The methods described in this work can be widely used in determining the elastic properties of thin films and artificial SEIs.

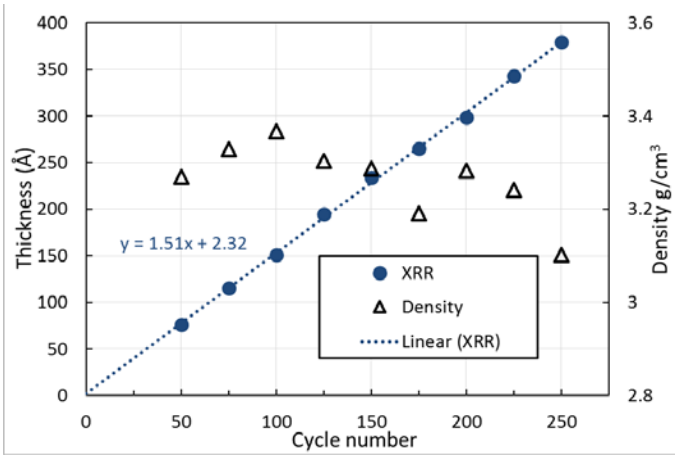

Figure 4.1 Thickness of ALD Al_2O_3 films. The thicknesses correspond to 50 to 250 reaction cycles and varies from 7.6 nm to 37.9 nm as determined by XRR (filled circles). The growth rate is 1.51 Å /cycle (constant growth rate). Dashed line corresponds to the fit results to the XRR thickness data; triangles are measured density by XRR for all films, with an average density is 3.26 g/cm3; the density does not change much with the thickness/cycle number.

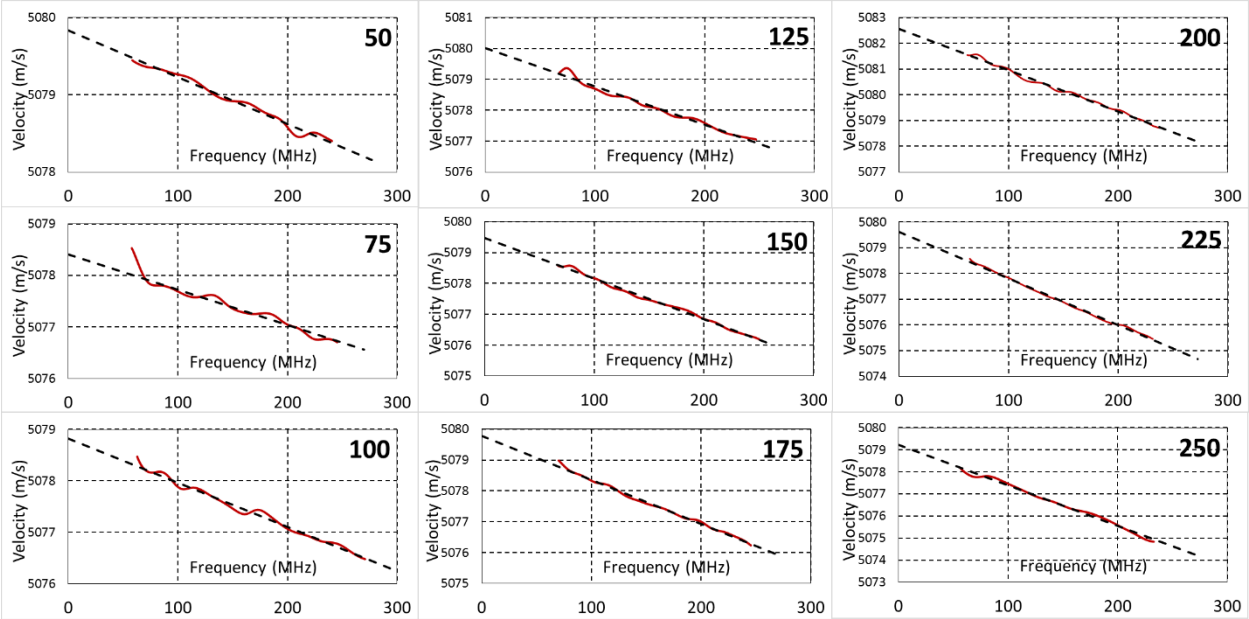

Figure 4.2 Dispersion curves (phase velocity versus frequency) for alumina-ALD samples: solid-lines are LAW data; dashed lines are model fits; and the reaction cycles are shown in upper-right corner of each figure.

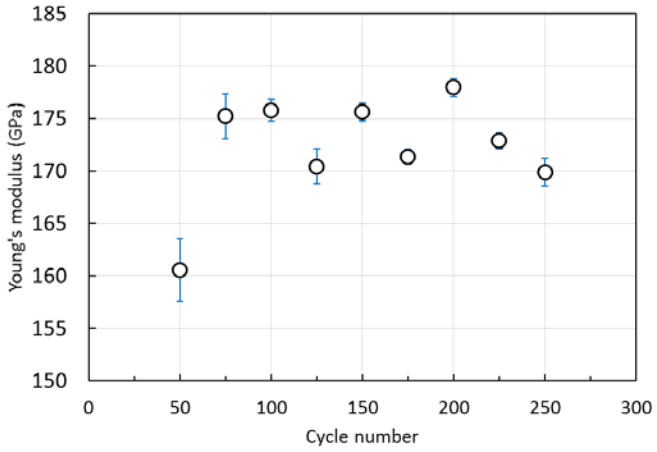

Figure 4.3 Young's modulus obtained from LAW. Except the thinnest film, 50 cycles (7.6 nm), the modulus is similar for all films and varies from 170 to 180 GPa.

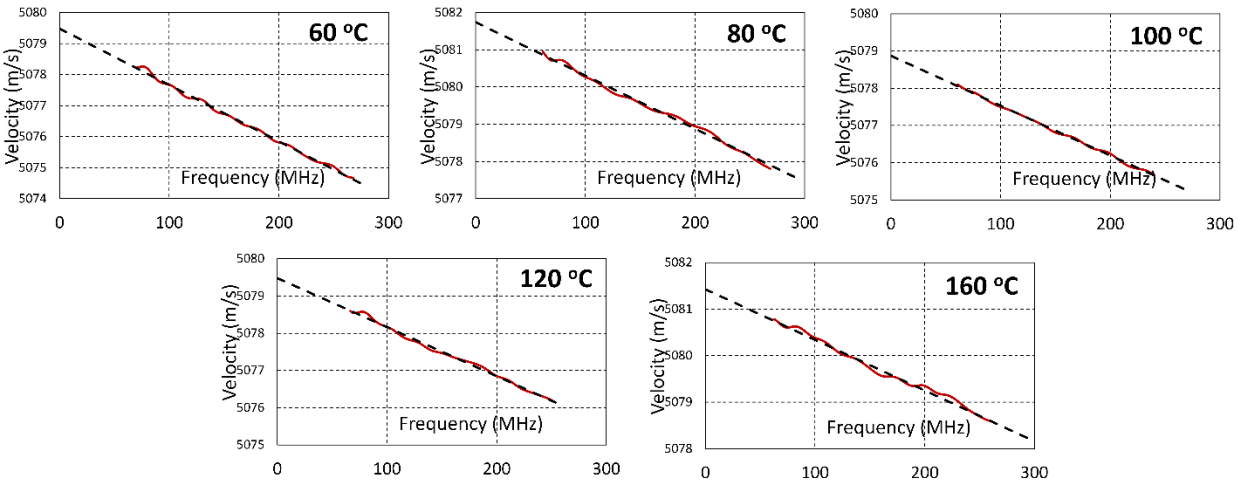

Figure 4.4 Dispersion curves (phase velocity versus frequency) for alumina-ALD samples: solid-lines are LAW data; dashed lines are model fits; and the disposition temperatures are shown in the upper-right corner of each figure.

Table 4-1 Summary of the properties of different ALD alumina films.

Cycle number	Thickness (nm)	Growth rate (Å/s)	Density (g/cm^3)	E (GPa)
250	37.91	1.52	3.10	171.22±1.04
225	34.29	1.52	3.24	172.86±0.72
200	29.84	1.49	3.28	177.96±0.88
175	26.53	1.52	3.19	171.34±0.68
150	23.37	1.56	3.29	175.63±0.88
125	19.45	1.56	3.30	170.42±1.67
100	15.09	1.51	3.37	175.76±1.05
75	11.49	1.53	3.33	175.21±2.15
50	7.62	1.52	3.27	160.56±2.96

Table 4-2 Area density measurements of the Al_2O_3 coating as determined by EPMA quantitative measurements and GMRFILM thin film modeling program using scanning mode (30 μm area).

Position	Area density ($\mu g/cm^2$)
1	11.9
2	11.7
3	11.7
4	11.6
5	12.0
6	12.1
7	11.6
8	11.7
9	11.7
10	11.6
Average	11.8
Std. dev.	0.2

Table 4-3 Summary of Young's modulus of different alumina ALD film in literature and this work.

Deposition temperature (°C)	Thickness (nm)	Testing method	Young's Modulus (GPa)	Reference
300	60	Nanoindentation*	220±40	[81]
177	300	Nanoindentation	180±8.2	[82]
177	100	Nanobeam deflection	168±8	[82]
177	50	Nanobeam deflection	182±32	[82]
120	**7.62**	**LAW**	**160.56±2.96**	**This work**
120	**11.5-38**	**LAW**	**170-180**	**This work**
100	300	Nanoindentation	150-155	[88]

*Continuous stiffness method combined with simulation results

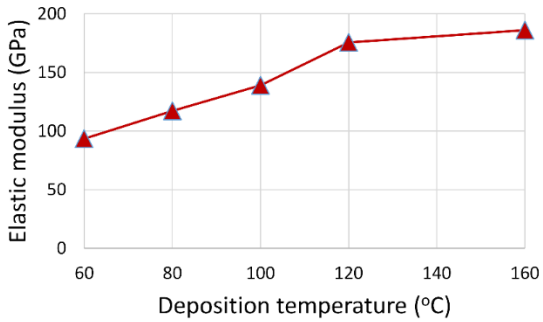

Figure 4.5 Elastic modulus of different ALD films prepared under different deposition temperature. The moduli range from 90 to 190 GPa.

Table 4-4 Summery of the properties of different ALD alumina films deposited under different temperature.

Cycle Number	Deposition Temperature (°C)	Thickness (nm)	Density (g/cm^3) [Estimate]	Elastic Modulus (GPa)
150	60	20.71	2.48	93.56 ± 0.99
150	80	20.06	2.64	117.28 ± 1.24
150	100	23.37	2.88	139.13 ± 0.92
150	120	20.63	3.29	175.63 ± 0.88
150	160	20.77	3.4	186.18 ± 0.11

Chapter 5. Design the Artificial Solid Electrolyte Interphase by Utilizing the Synergetic Effects of Inorganic Components to Facilitate the Ionic Transport and Reduce the Electrolyte Decomposition[3]

5.1. Summary

As previously discussed in Chapter 3, there are two important inorganic components identified: lithium fluoride and lithium carbonate. It is well known that LiF is a good electron insulator. Although lithium carbonate and lithium fluoride have relatively low ionic conductivity, we found that a composite coating made of both components creates a defective interface with space charge, which significantly improved lithium ion transport. The synergetic effect of both inorganic components lead to high current efficiency and cycling stability. We envision that the defective composite coating is a promising artificial solid electrolyte interphase (SEI) layer to suppress the undesirable side reactions and improve the life of lithium ion batteries employing silicon negative electrodes.

5.2. Introduction

Lithium ion batteries (LIBs) have been the choice for many electrochemical energy storage systems, including portable electronic devices, uninterruptible power supplies (UPSs), and electrical vehicles (EVs).[89, 90] High energy and power density, along with durability are three key goals for developing advanced LIB systems. (Note: cost and recharge time are also important.) Silicon has been considered as the next generation negative-electrode material due to its highest theoretical specific capacity (over 3600 $mAhg^{-1}$) by forming $Li_{15}Si_4$. [15-17] However, silicon electrodes have poor durability, caused by the mechanical degradation originated from the huge volume change while cycling.[23] In order to meet the desired ultra-long life requirements for EV applications, much research has been devoted to stabilizing the electrodes for LIBs. One of the promising approaches is to reduce the Si particle size to achieve better mechanical

[3] Reproduced from *Qinglin Zhang, Jie Pan, Peng Lu, Mark W Verbrugge, Brain W Shelton, Yang-Tse Cheng, Yue Qi and Xingcheng Xiao, "Synergetic Effects of Inorganic Components in Solid Electrolyte Interphase on High Cycle Efficiency of Lithium Ion Batteries," **Nano Letters**, 16 (3) : 2011-2016 (2016)*

integrity during cycling. [15, 32, 91, 92] However, nanosized silicon particles have high surface area exposed to the electrolyte, forming large amounts of SEIs.[35, 93] The SEI is a passivation layer formed on the electrode surface that is critical for stabilizing lithium ion battery electrodes. However, the formation of SEI on negative electrodes consumes Li irreversibly in Li-ion cells. The unstable SEI on electrode surface, caused by the Si volume changes during lithiation and delithiation, leads to low cycling efficiency and irreversible capacity loss. Therefore, stabilizing the SEI is of great interest to the research community for Si electrodes. [93]

Intensive research efforts have been devoted into studying the properties of the SEI and stabilizing the SEI by electrolyte additives, surface modification and geometric design.[25, 36, 37, 94] Our previous study has revealed the relationships among the structure, property, and cycling performance of naturally formed SEI. Typically, an SEI layer with a high modulus can provide better mechanical protection, leading to higher cycle efficiency and improved capacity retention. [93]

In a naturally formed SEI, inorganic components are concentrated near the electrode surface and organics on the top of inorganics. There are three major components in naturally formed inorganic SEI: lithium carbonate, lithium oxide and lithium fluoride.[93, 95] These lithium containing components play important roles in mechanically stabilizing the SEI. In the past, several inorganic coatings, including oxides, carbonates, and fluorides, have been developed as the artificial SEI to stabilize the electrode. These individual components have been shown to yield different electrochemical behavior as well as different transport properties. [28, 94, 96, 97]

The ionic and electronic transport through the artificial SEI depends on the defect chemistry in the multi-component SEI coated on electrodes. On one hand, the dominant defect type in a pure LiF coating on anodes is a Schottky pair (cation and anion vacancy pair).[98] It has been reported that LiF is a good electronic insulator (~10^{-31} S/cm) but has a poor ionic conductivity.[98] On the other hand, the main defect in Li_2CO_3 is Li ion vacancy with its charge balanced by free electrons.[99] As a result, Li_2CO_3 can provide relatively higher ionic conductivity (~10^{-8} S/cm) but maintains a considerable electron concentration on negative electrodes.[100] Either one of them alone will not work, but

they appear to work in a combined way, likely for the reasons just described, and similar with naturally-formed inorganic SEI.

In order to identify the role of different components in the SEI systems and explore the optimum composition of SEI which can effectively passivate Li-ion battery electrodes and facilitate the Li ion transport, we designed the artificial SEI with the aforementioned three inorganic components co-existing in the naturally formed SEI on silicon thin film electrodes. Silicon thin film electrodes provide a good platform to investigate the functions of artificial SEI layers: they can avoid the severe mechanical degradation compared with silicon particles, avoiding the impact of newly formed SEI associated with surface damage. The relatively smooth and well defined surface enables us to carry out well-controlled and unambiguous chemical and mechanical characterization using many surface sensitive techniques.

5.3. Experimental Section

Si thin-film electrodes (~100 nm) were prepared by RF magnetron sputtering on copper current collectors, and tested in coin cells for electrochemical characterizations. Surface coatings were also prepared by RF magnetron co-sputtering of lithium fluoride and lithium carbonate targets on as-prepared Si thin-film electrodes. The ratio of the coating materials was controlled by the sputtering rate (power control).

The Si electrodes (or coated Si electrodes) were used as working electrodes, and pure lithium metal foil as counter and reference electrodes in CR2032 coin cells. A separator (Celgard, USA) was placed between working electrode and lithium foil, and 1M $LiPF_6$ in ethylene carbonate and dimethyl carbonate (EC:DMC 1:1 volume ratio, BASF) was employed as the electrolyte. The Arbin battery test system (BT-2000) was used to cycle the coin cells, using the constant-current method (with a rate of C/3) and a voltage window between 0.05 V to 1.5 V. The electrochemical impedance spectroscopy (EIS) study was conducted in two-electrode coin cells at the assigned voltage. The coin cells were rested for 24 hours until they were stabilized.[46] The high-frequency (Ohmic) resistance of the coin cells ranged from 400 to 500 Ohms. The applied frequency range

for EIS measurements was between 1 MHz to 10 mHz by a VMP3 potentiostat (Biologic).

Thermo Scientific K-Alpha X-ray photoelectron spectroscopy (XPS) with a monochromated Al Kα source (1486.6 eV) was used for chemical analysis of coatings and the SEIs on the electrodes. Transmission electron microscopy (TEM) sample was prepared by FEI Helios Nanolab 660 dual beam focused ion beam (FIB), and high-resolution TEM pictures were taken by JEOL 2010F under an acceleration voltage of 200 kV.

For the isotope exchange experiment, the as-prepared LiF/Li_2CO_3 thin films (of three compositions, <1% LiF, 15% LiF, and 50% LiF) were soaked in 0.1M $^6LiClO_4$ (95% ^6Li abundance, $^6Li^+/^7Li^+ \sim 20$) dimethyl carbonate solution in an Ar glove box for 3 min. After the immersion, the specimens were rinsed thoroughly with dimethyl carbonate (DMC), dried in the glove box, and transferred under Ar in a special vessel to the analysis instrument.

The time-of-flight secondary ion mass spectrometry (TOF SIMS) analyses were performed on a PHI TRIFT V nanoTOF spectrometer (Physical Electronics, Chanhassen, MN). The analysis chamber of the instrument was maintained at a pressure of less than 5×10^{-7} Pa during the analyses. A 30kV Au^+ ion source was used for both sputtering and analysis. The analysis area was 50 μm × 50 μm, within a sputter area of 200 μm × 200 μm. A uniform sputter rate of 0.1 nm/s (calibrated with 100 nm SiO_2) was used to calculate the sputter depth.

5.4. Results and Discussion

By controlling the power of each RF source, the deposition rate of Li_2CO_3 and LiF will change accordingly, allowing on to modulate the final composition of artificial SEI films (cf. Figure 5.1). The deposited artificial SEI films have been characterized by XPS. Figure 5.2 shows the depth profiles of different artificial SEI films. Obviously, SEI1 has the highest concentration of F. The atomic percentage of F is around 15%. If counting the

films as Li_2CO_3/Li_2O and LiF (by molar), half of the inorganic components are LiF. SEI2 and SEI3 contain 15% and <1% of LiF, respectively, as shown in Table 5-1.

XPS was also carried out on the artificial SEI films after cycling. From the XPS spectra (Figure 5.3), we can see that the composition of artificial films remain unchanged, and the concentration of each element/species is kept the same (see Figure 5.4 for the depth profile). This is an indication that artificial SEI films are stable upon cycling.

Coulombic efficiency is an important indictor on the prediction of cycle life for Li-ion battery electrodes, especially when evaluating the performance in full-cell. In Li-ion full cells, usually the Li is brought into the cell with the new (air-stable) lithiated cathode (e.g. $LiCoO_2$, $LiFePO_4$); this fixes the amount of Li available for cell electrochemical operation. Any irreversible Li reaction will cause permanent capacity loss of Li-ion cells. Thus, Coulombic efficiency measurement can often be used as an indicator of irreversible Li loss during each cycle. High Coulombic efficiency is essential for durable Li-ion cells.[101] Figure 5.5 shows the comparison of Coulombic efficiency of Si electrodes with different artificial SEI coatings. The cells were tested without any electrolyte additives. All the artificial SEI coated Si samples show improved Coulombic efficiency, improved from an average of 98.46% (bare Si) to 99.43% (SEI1), 99.27% (SEI2) and 98.95% (SEI3). For the first cycle, Coulombic efficiency was improved by applying the artificial SEI coatings. The first cycle Coulombic efficiencies are 81.81% (bare Si), 88.15% (SEI1), 88.78% (SEI2), and 84.99% (SEI3). The decreasing of general trends of Coulombic efficiency can be attributed to the mechanical degradation of Si thin film electrodes. Figure 5.5 also shows the capacity retention for different samples. SEI1 has the best capacity retention. In order to correlate the mechanical properties of artificial SEIs with performance, we measured the hardness and elastic moduli of different SEIs by nanoindentation, as shown in Table 1. Among all three artificial SEI films, SEI1 has the highest modulus and hardness, which are 86 GPa and 2.2 GPa, respectively. Previous study shows that the elastic properties of SEIs can impact the cycling performance. The elastic properties of SEIs can influence the energy barrier for crack nucleation and propagation, and the generation of cracks is one of the major causes for low Coulombic efficiency and capacity degradation. Low Coulombic efficiency is caused by forming

new SEI on the cracks, and permanent capacity loss is due to lithium consumption at the interface, and the isolation of the electrode material, and loss of electrical contact between regions of otherwise active material.

The rate testing was also performed on Si electrodes with different SEI coatings, as shown in Figure 5.5. Under low rate (C/5 or C/3), all the Si electrodes behave similarly. When cycling the cells at higher rates, Si electrodes with SEI 1 coatings have the highest capacity, and bare Si electrodes show the lowest capacity. Compared with bare Si electrodes, all the artificial SEIs enhance the rate capability. This is an indication that the coated SEI layers are better than that which is naturally formed, with SEI1 providing the best rate capability, consistent with SEI1 having promoting the fastest ionic transport.

Figure 5.6 right shows the typical EIS recorded for Si electrodes with different artificial SEIs (at 0.6 V immediately after lithiation) in Si/Li half cells. The typical EIS spectra comprised two semi-cycles in medium frequency range. It is generally accepted that the first semi-cycle at higher frequency originates from interfacial resistance (R_{int}) and the semi-cycle at lower frequency originates from charge-transfer process. The lower frequency tale of EIS spectra corresponds to semi-infinite diffusion, or Warburg resistance.[46] The EIS results show that even for Si thin films coated with thick artificial inorganic SEI layers, the overall impedance is not greatly affected. We fit the first semi-circle of EIS spectra to get the interfacial resistance (R_{int}). Figure 5.6 (right) shows an example of fitting and the equivalent circuit (embedded).[102] Figure 5.6 (left) shows the fitting results of voltage depended R_{int} of different artificial SEI samples. The general trends of R_{int} are the same for all the samples: R_{int} started a drop when discharged (lithiated) from 0.4 V to 0.2 V for Si samples coated with SEI1, 2 and 3, and from 0.6 V to 0.2 V for Si samples without coatings. The R_{int} drop corresponds to the irreversible process during galvanostatic cycling. [103] The R_{int} for bare Si, Si coated with SEI1, 2, 3 are 305, 196, 302, 225 ohm respectively. After stabilization, SEI1 has the lowest R_{int} value (around 200 ohm).

The underlining reason for promoting the total ionic conduction by introducing LiF into Li_2CO_3 as a composite artificial SEI is the formation of LiF/Li_2CO_3 interface. Figure 5.7(a) shows the high resolution TEM images on all three artificial SEI coatings show

mixed LiF, Li_2O and Li_2CO_3 nanocrystals, with randomly orientated interfaces. TEM characterization identified three phases: 1) nanocrysalline LiF, 2) nanocrystalline Li_2O, and 3) amorphous and poorly-crystalized Li_2CO_3. Li_2CO_3 is known to be unstable during TEM sample preparation with a low dissociation barrier, which is easily to be decomposed to Li_2O and CO_2.[104-106] SEI 1 structure characterized by high resolution transmission electron microscopy (HRTEM) and selected area electron diffraction (SAED). Figure 5.7 (a) shows a typical HRTEM image of the SEI 1, showing nanocrystals (2 - 5 nm in size). The inset is an SAED pattern taken from the SEI 1. The SAED pattern shows a diffraction halo and multiple diffraction rings. Figure 5.7 (b) shows the profile of the highlighted box in (a) which is obtained by converting the 2-dimensional diffraction pattern into 1-dimensial spectrum to show the positions of diffraction peaks. Peak 1 (the broad peak at 3.79 Å) is the diffraction halo and corresponds to the $(\bar{1}11)$ of Li_2CO_3. This indicates Li_2CO_3 is an amorphous phase. Peaks 2 at and 6 uniquely belong to the (111) and (113) of LiF; and Peak 4 uniquely to the (022) of Li_2O. The rest peaks (3 and 5) can be an overlap of both LiF and Li_2O due to their close atomic plane distance (i.e., d-spacing). Figure 5.7 (c) shows the colored and zoomed-in SAED pattern (for better visualization) showing the diffraction halo. Figure 5.7 (d) shows a typical HRTEM image, showing the poor crystallinity of the $(\bar{1}11)$ of Li_2CO_3. The HRTEM shows the coexistence of both Li_2CO_3 and LiF, and there are huge around of interface between them.

The simulation result shows that, the defects concentration at the interface between Li_2CO_3 and LiF has been significantly promoted in Li_2CO_3 by introducing LiF, and generating the Li_2CO_3 and LiF interfaces, as shown in Figure 5.8.

In order to correlate the electrochemical performance and simulation results, we carried out the isotope ion-exchange experiments to investigate the effect of interface between two phases. Figure 5.9 compares the isotope ratio $^6Li^+/^7Li^+$ verse depth profile measured by ToF-SIMS after 3 min of $^6Li^+$ ion exchange. The $^6Li^+/^7Li^+$ ratio becomes almost constant in the top coating layer for all three SEIs. However, the ratios are significantly different among these samples. The higher ratio means higher $^6Li^+$ exchange, which is an

indication of faster Li^+ transport. The simulation in the previous section shows that LiF has fewer charger carriers than Li_2CO_3. However, by adding LiF into Li_2CO_3, the rate of Li ion exchange in fact increases. Apparently, the mixing of Li_2CO_3 and LiF creates more interfaces between Li_2CO_3 and LiF, leading to more ion exchange in those regions. The results are consistent with the rate capability test shown in Figure 5.5.

5.5. Conclusion

Engineered multi-component inorganic SEIs consisting of LiF and Li_2CO_3 have been successfully applied on thin film Si electrodes. The properties and performance of these electrodes support the following conclusions: (1) LiF is a critical component in SEI for stabilizing the SEI layer and improving the cycling efficiency; (2) The synergetic effects of LiF and Li_2CO_3 interfaces, which not only facilitate Li ion transport, but also further enhance the passivation function to suppress electrolyte decomposition. We envision this work can be beneficial in helping design the surface coatings/electrolyte additives for Li-ion cells, hence improving the durability of Li-ion battery electrodes.

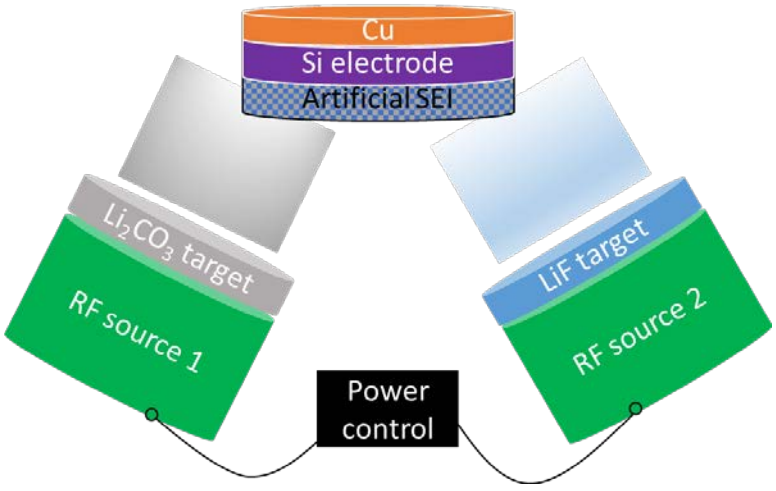

Figure 5.1 Illustration of co-sputtering process to form the artificial SEI coatings on Si

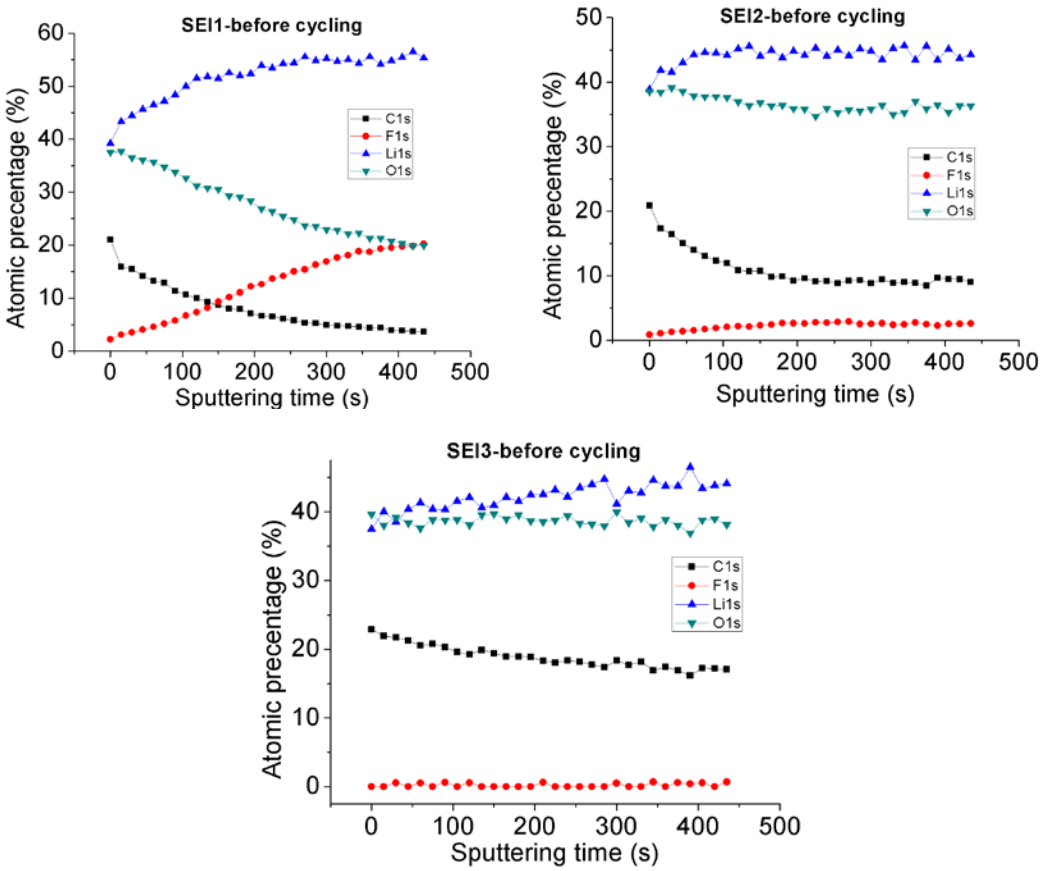

Figure 5.2 XPS depth profile for different SEI films before cycling.

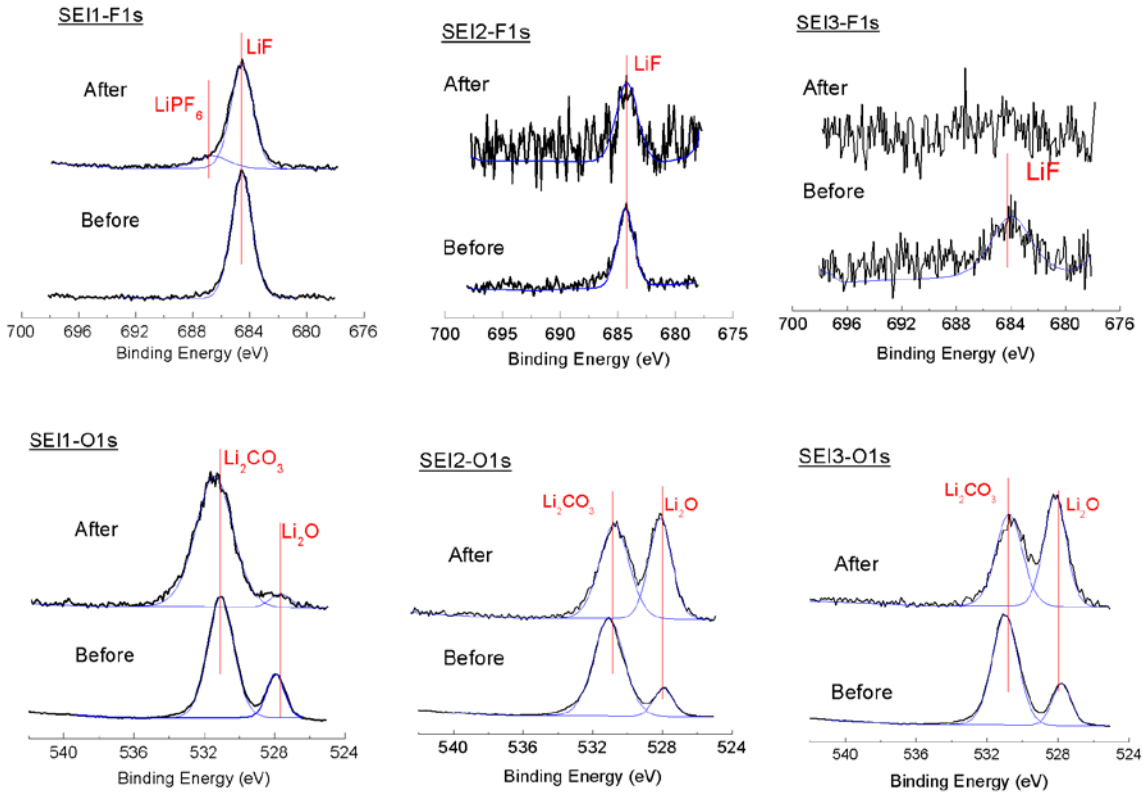

Figure 5.3 XPS spectra of SEI 1, 2 and 3, before and after cycling

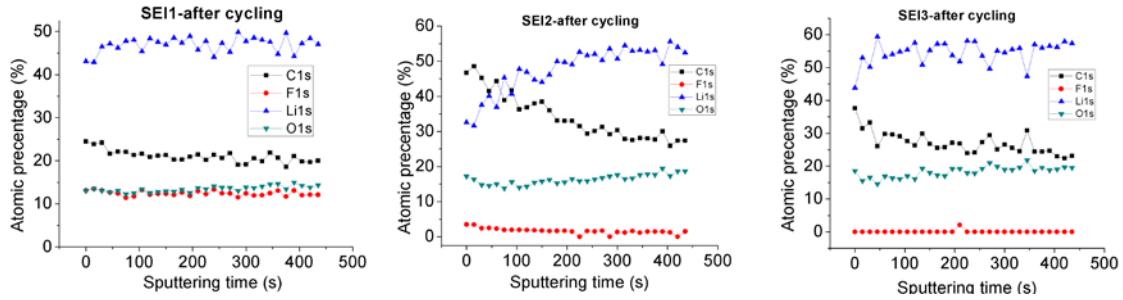

Figure 5.4 XPS depth profile for different SEI films after cycling.

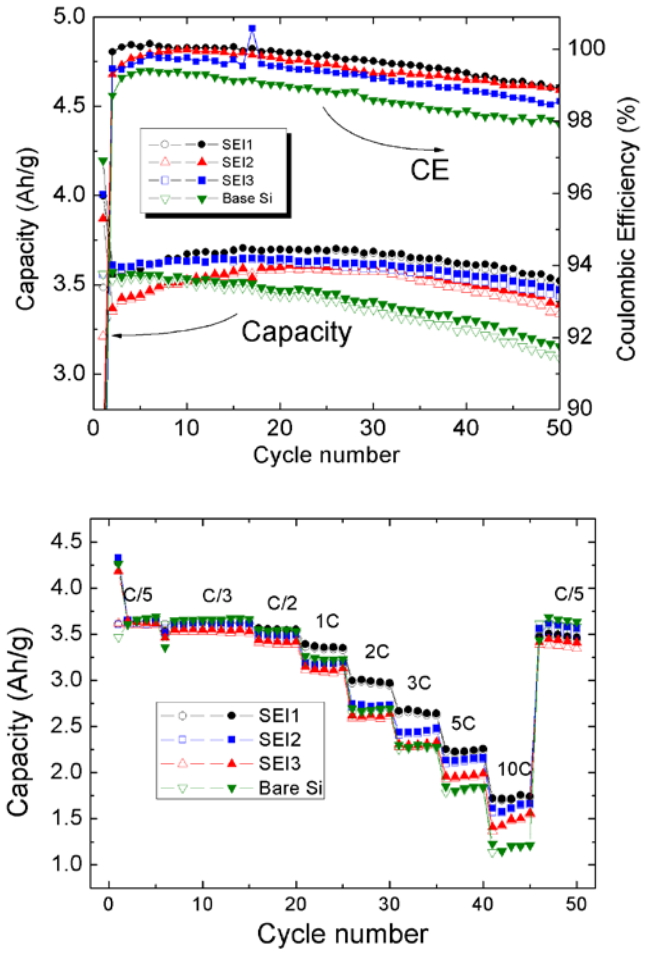

Figure 5.5 (above) Capacity, Coulombic efficiency (upper plot) and rate capability (lower plot) of Si electrodes with different artificial SEI coatings; SEI1 has the highest LiF content.

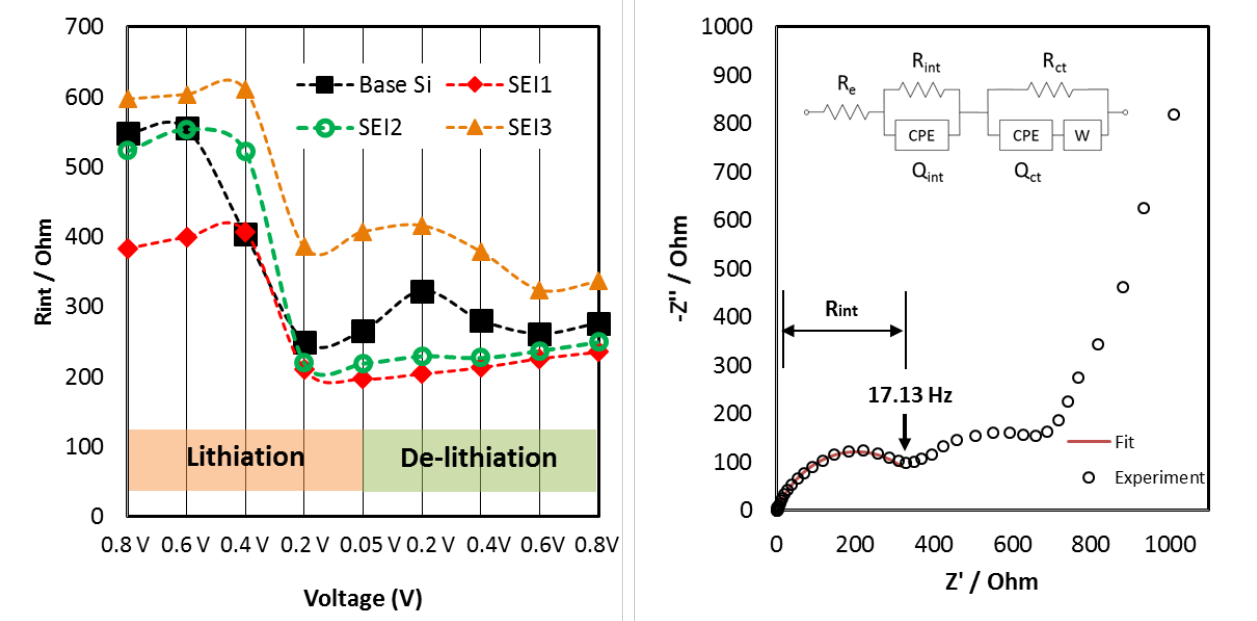

Figure 5.6 Left: Interfacial resistance (R_{int}) of different samples under different lithiation (de-lithiation) stage. Right: example of fitting of interfacial resistance at medium frequency range (at 0.05 V).

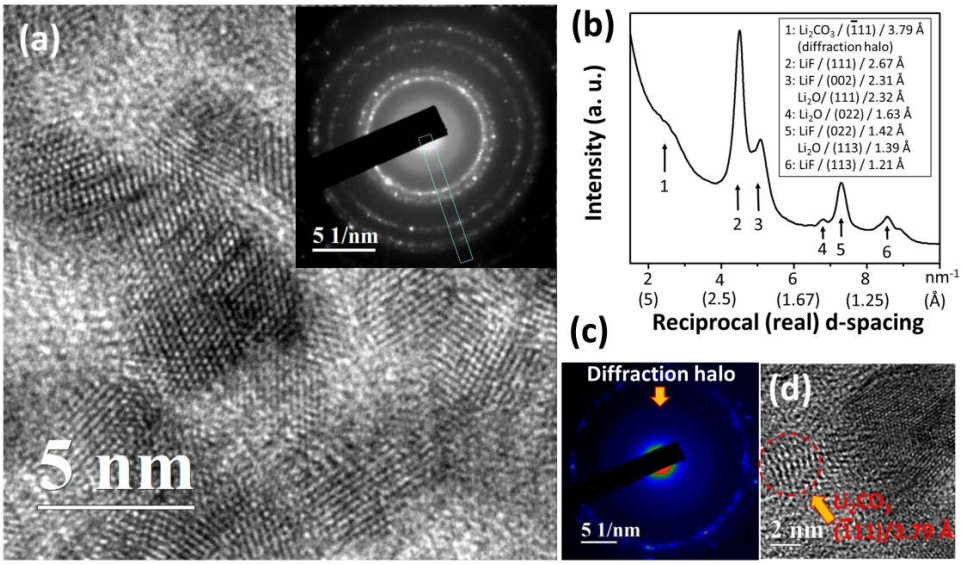

Figure 5.7 High resolution transmission electron microscopy (HRTEM) image and selected area electron diffraction (SAED) of SEI1: (a) A typical HRTEM image, the inset is an SAED pattern; (b) Profile of the highlighted box in (a) which is obtained by converting the 2-dimensional diffraction pattern into 1-dimensial spectrum to show the positions of diffraction peaks. (c) Colored and zoomed-in SAED pattern (for better visualization) showing the diffraction halo. (d) An HRTEM image showing the poor crystallinity of the ($\bar{1}$11) of Li_2CO_3

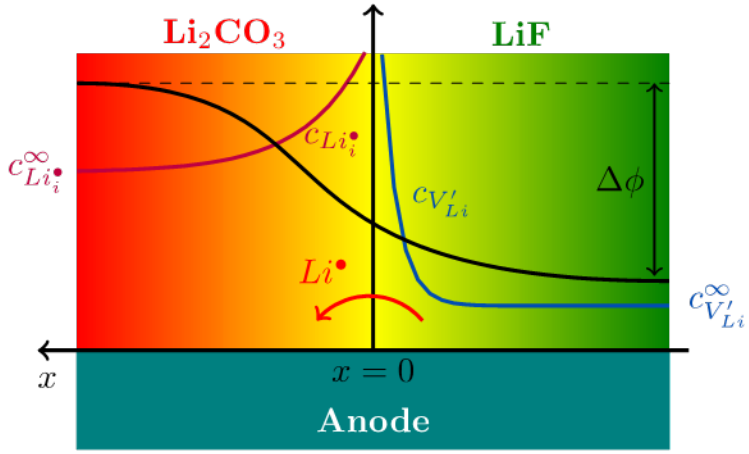

Figure 5.8 Schematic figure showing the defect reaction[$Nil \rightarrow Li_i^{\cdot}(Li_2CO_3) + V'_{Li}(LiF)$] and defect distribution near the LiF/Li_2CO_3 interface (bulk defect concentration [98, 100]: $c^{\infty}_{Li_i^{\cdot}} \approx 10^{15}\ cm^{-3}, c^{\infty}_{V'_{Li}} \approx 10^{-2}\ cm^{-3}$).

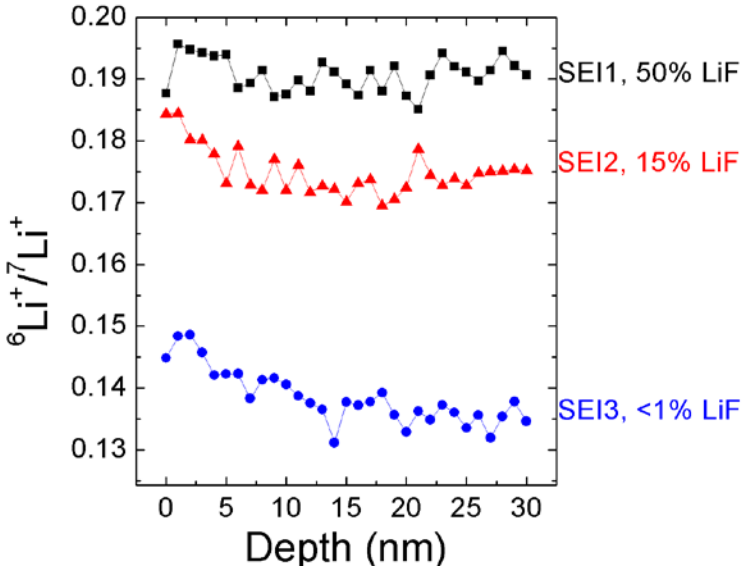

Figure 5.9 TOF-SIMS results of the ratio between ^{6}Li and ^{7}Li, after 3 min of ^{6}LiClO solution soaking.

Table 5-1 Composition of different artificial SEIs before and after cycling

Artificial SEI	**Estimate thickness**	**F atomic percentage before cycling**	**F atomic percentage after cycling**	**Approximate LiF percentage (counts as LiF, Li_2CO_3 and Li_2O)**
SEI1	100 nm	15%	15%	50%
SEI2	100 nm	4%	3%	15%
SEI3	100 nm	<1%	<1%	<1%

Table 5-2 Mechanical properties of different SEI films, obtained by nanoindentation

	Hardness (GPa)	**Modulus (GPa)**
SEI1	2.22 ± 0.10	86.43 ± 1.28
SEI2	1.02 ± 0.08	63.73 ± 3.49
SEI3	0.65 ± 0.07	25.92 ± 1.05

Chapter 6. A Chemically Stable Artificial Solid Electrolyte Interphase: Hafnium Oxide Coatings by Atomic Layer Deposition

6.1. Summary

The importance of coating's chemical stability has been demonstrated by this study. It is well known that the mechanical properties determine the cycle life, and chemical stability or chemical degradation rate determines the calendar life. In this study, we used HfO_2 atomic layer deposition coatings as an example to show the chemical stability of the coatings for lithium ion battery electrodes.

6.2. Introduction

Lithium ion batteries (LIBs) have been the choice of energy storage systems for portable electronic devices, uninterruptible power supplies and electrical vehicles. Exploring novel electrode materials with higher capacity, better rate capability, longer life and lower cost is in urgent need for using LIBs in wider applications. For example, Si electrode is able to deliver over 3600 mAh/g capacity, but the cycle and calendar life is not desirable due to both intrinsic issues of electrodes (such as large volume change) and surface chemical instability.[23, 107-111]

Mechanical and chemical degradation are two major degradation mechanisms of most LIBs. Usually, the cycle life is determined by the mechanical degradation rate; and the calendar life is determined by the rate of chemical degradation. [101] The stability of the electrode-electrolyte interphase, or solid-electrolyte interphase (SEI) in non-aqueous electrolyte is critically important for stabilizing the electrodes and enabling the long-term cyclability.[112-119] The stability of SEI can significantly influence the life of LIBs. Intensive research efforts have been devoted to designing the SEI by incorporating electrolyte additives, such as FEC, VC, and LiBOB.[120-127] These electrode additives can help form stable SEIs on electrodes to prevent further decomposition of electrolytes. Even with the additives, however, the formation of SEI is still a Li consuming process, which causes irreversible Li loss (or capacity loss) during the formation cycles.

In addition to electrolyte additives, surface coatings have been employed to improve the functionalities of electrodes.[28, 94, 128, 129] There are many advantages of surface coatings, such as reducing the irreversible capacity loss, improving the kinetics of electrodes and better control of SEI layers.[94, 130] The surface coatings, or artificial SEIs (a-SEIs), need to be electronic insulating (suppress the electrolyte reduction), Li ion conducting, and chemically stable. [112]

Recently, several coatings made by atomic layer deposition (ALD) have been demonstrated to be effective a-SEIs to protect the electrodes. There many advantages of ALD , such as the film was deposited under a relative low temperature with controllable thickness of atomic precision, good stoichiometric, excellent uniformity and conformity. [28, 55, 56, 131, 132] TiO_2, Al_2O_3, ZnO_2, SnO_2, and SiO_2 coatings are used as protection layers for both cathodes and anodes of LIBs.[59, 133-135]

In this work, we introduce the HfO_2 as a-SEI to stabilize Si electrodes. Hafnium oxides have been widely used as high-*k* dielectrics in semiconductor industry due to its good electronic insulating capability. Moreover, HfO2 is known for its stability under various conditions, [136-138] which may be desirable for LIB applications. We use x-ray photoelectron spectroscopy (XPS) to demonstrate the stability of HfO_2 coatings by comparing the cycle-aged electrode coatings with freshly prepared coated electrodes. The results show that, unlike other coatings that change their chemical compositions after cycling, HfO_2 coatings maintain chemically stability, hence improving the cycling stability of the Si electrode significantly.

6.3. Experimental Details

Silicon thin film electrodes were deposited on a copper current collector by RF magnetron sputtering. The sputtering rate was 0.1 nm/s, and the thickness was controlled to be 100 nm.

Atomic Layer Deposition (ALD) has been used to grow metal oxide thin films with uniform chemical composition and precisely controlled thickness because of ALD's self-limiting growth mechanism. Thin films with consistent quality can be grown by ALD

conformally on a variety of substrates, including substrates with high aspect-ratios, rough and porous, which tremendously broadens the application field of ALD [139-142]. In the present work, HfO_2 was deposited on Si electrodes and wafers using ALD (Cambridge NanoTech, Inc.) at 300°C. The Hf atoms were provided by the amide precursor tetrakis(dimethylamido)hafnium (TDMAH), and the oxidant was H_2O. TDMAH and H_2O were supplied sequentially into the ALD chamber with TDMAH supplied first. TDMAH was heated up to 75°C to provide a high enough vapor pressure. The nitrogen carrier gas was provided at a flow rate of 20 sccm (standard cubic centimeters per minute). The pulse time of 20 seconds was long enough to meet the saturation requirement of each ALD cycle. After deposition of HfO_2, a multi-angle Spectroscopic Ellipsometry (J. A. Woollam M3000 V) was used to measure the coating thickness and optical constants (refractive index, n, and extinction coefficient, k) of the thin HfO_2 films.

Si and HfO_2 coated Si electrodes were used as working electrodes. Lithium metal foil was used as counter and reference electrode. CR 2025 coin cells were assembled in the Ar filled glovebox with control of oxygen and moisture concentration below 0.1 ppm. Microporous membrane (Celgard 3501) was used as the separator. 1M $LiPF_6$ in ethylene carbonate and diethyl carbonate (EC:DEC 1:1 volume ratio, BASF) was used as the electrolyte. The Biologic VMP3 was used to cycle the coin cells between 1.2 and 0.05 V vs. Li/Li^+ under a charge/discharge rate of C/3 (1C corresponds to 3600 mA/g). The electrochemical impedance spectroscopy (EIS) was conducted in two-electrode coin cells at assigned voltages. The coin cells were rest for 24 hours until stabilized before EIS measurements. The frequency range applied was 1MHz to 10 mHz. The fitting of equivalent circuit was performed using the EC-Lab software (Biologic).

A Thermo Scientific K-Alpha XPS system with a monochromatic Al Kα source (1486.6 eV) was used for chemical analysis of coatings and SEIs on the electrodes before and after cycling. The post-cycled electrodes were harvested from the dissembled coin cells, washed with DMC in the Ar-filled glovebox before transferring to the XPS analysis chamber. The transferring process was completed by a specially designed air-tight transfer holder to avoid sample exposure to air.

6.4. Results and Discussion

During the deposition, a Si wafer was placed adjacent to the Si electrodes in the ALD reaction chamber. The as prepared HfO_2 film on the Si wafer was characterized by ellipsometry to confirm the thickness. The measured thickness for 20 layers of HfO_2 is 25.09±0.0226 Å, corresponding to 1.25 Å per layer. The thickness matches well with previous studies of HfO_2 growth. [81, 138, 139]

Figure 6.1 shows the cycling performance of bare Si electrodes, Si coated with 5 layers (0.63 nm), 10 layers (12.5 nm) and 20 layers (25.1 nm) of HfO_2 under the constant current with a charge/discharge rate equivalent to C/3 (C = 3600 mA/g). Figure 6.1 (a) shows capacity retention. The first cycle discharge capacity is about 3600 mAh/g, then stabilized around 2800 mAh/g for all samples. After 100 cycles, the Si electrode coated with 20 layers of HfO_2 shows 2019.58 mAh/g capacity, with 70.1% capacity retention. In comparison, the bare Si electrode without coating only show a capacity of 1331.73 mAh/g after 100 cycles, with 45.9% capacity retention. The Si electrodes coated with 5, and 10 layers of HfO_2 show improved performance, but not as good as that of 20 layers. The Coulombic efficiency (CE) is an important indicator to evaluate the performance of LIB electrodes. Figure 6.1 (b) shows the CE of different samples. The first cycle CE was 68.3%, 79.7%, 78.6% and 78.5% for bare Si electrode, with 5, 10 and 20 layers of HfO_2 coatings, respectively. The low first cycle CE can be attributed to the formation of SEI on the electrodes and stainless steel conducting coin-cell cases. The results show that, with the HfO_2 coatings, the first cycle CE has been improved, due to the suppressed formation of SEI on the electrodes. The CE for coated samples raised above 99% during the first 20 cycles, in comparison with bare Si samples, which is lower than 99%. The majority of the reactions during SEI formation is caused by electrolyte reduction. The improved CE for coated samples indicates that, compared with naturally formed SEIs, HfO_2 coatings can be a more effective in blocking the electrons from contributing to electrolyte reduction reactions.

To characterize the kinetic properties of the coated Si electrodes, EIS was carried out before and after cycling. Figure 6.2 shows the Nyquist plots of impedance spectra

recorded for bare Si electrodes and Si coated with HfO_2 coatings at open circuit potential, before and after cycling. The semi-circle (at high frequency region) originates from the interfacial resistance (R_{int}). The low frequency tail of EIS spectra corresponds to the semi-infinite diffusion, or Warburg resistance.[46] By fitting the semi-circles, we obtained the interfacial resistance which is given in Figure 6.2. For the fresh electrodes before cycling, the HfO_2 coatings can significantly reduce the R_{int} from 600 Ohm (bare) to 200-300 Ohm (coated). We also compared the R_{int} after 10 cycles, when the surface passivation has been stabilized. After 10 cycles, Si electrodes coated with 20 layers of HfO_2 has the lowest R_{int} (71 Ohm), and compared with bare Si w/o coating, all HfO_2 coated samples show reduced R_{int} (100 Ohm for 5 layers of HfO_2, 79 Ohm for 10 layers of HfO_2 and 117 Ohm for bare Si electrodes). The increased resistance results in incomplete charge/discharge of the cells, especially when increasing the cycling rate.[143] The reduced R_{int} for 20 layers of HfO_2 coated on Si electrodes indicates that the HfO_2 coating reduces the R_{int} to more favorable values.

Figure 6.3 compares the cyclic voltammetry (CV) curves of bare Si electrode, and 20 layers of HfO_2 coated Si electrode for the 1st and 2nd electrochemical cycle. There are three reduction peaks for bare Si electrode in the 1st cycle: the peak around 0.5 V corresponding to the formation of SEI,[28] two peaks around 0.2 V and 0.1 V corresponding to Li insertion into Si electrodes. [110] [144] There are also two oxidation peaks during the reverse scan, corresponding to the Li extraction peaks, which match with the insertion peaks during the reduction scan. However, due to the irreversibility of SEI formation, there is no oxidation peak accounting for SEI formation. For the 2nd cycle, the majority formation of SEI is complete, therefore there are only two reduction peaks for Li insertion/extraction. For Si electrode coated with HfO_2, the identical SEI formation peak around 0.6 V does not appear, the SEI formation has been suppressed. This result can be correlated with the first cycle CE, which has been discussed in previous content. However, the first cycle reduction curve is not perfectly overlap with the 2nd cycle, which means that there is still some addition SEI formed, but the reactions are likely different from that on the bare Si electrodes. The analysis of the formation of SEI will be demonstrated in the next section on XPS analysis.

XPS was used to track the changes of HfO_2 coatings before and after cycling. Ar sputtering was used for depth profiling. Figure 6.4 (a) and (c) show the HfO_2 coated on the Si electrode before cycling; (a) shows that only Hf^{4+} was found on the top surface of the HfO_2 coating, (c) shows that both Hf^{4+} and metallic Hf^0 were found with longer sputtering time, and approached to the HfO_2 and Si interface. [145] There are two possible reasons for the existence of Hf^0 4f peaks: (1) the ion sputtering preferentially remove oxygen; and (2) metallic Hf is segregated to the Si/HfO_2 interface. [145] Figure 6.4 (b) and (d) show the Hf 4f XPS spectra of cycle-aged electrode. For both (b) and (d), we observed the similar peaks as that of fresh samples. Unlike other metal oxide ALD coatings, such as Al_2O_3, TiO_2 and SiO_2, HfO_2 coatings show good stability on Si electrode upon cycling. [28] Since the formation of LiMOx (M=Al, Ti, Si, etc.) is also a Li consuming process, the stability of HfO2 can help prevent additional Li loss during electrochemical cycling.

Figure 6.5 shows the depth profile of atomic percentage for the electrodes after cycling. Both electrodes show the existing of Li, O, P, C, F and Si elements, and HfO_2 coated sample shows, as expected, Hf signal. The Hf can be detected even after approximate 20 nm of sputtering, due to the surface roughness of Si thin-film electrodes. The low percentage of P2p means that the electrolyte has been cleaned by DMC thoroughly. The F signal is accounted for by the existence of LiF in the SEI. It is generally believed that LiF is favorable for improving the performance of Si electrode.[112, 125, 146] There is a higher F concentration for HfO_2 coated Si electrode, although the mechanism is still unclear. The percentage of Si is an indication of the thickness of SEI: the more Si detected corresponding to less SEI founded at the detected depth level. In our experiment, the detection of Si on HfO_2 coated sample increased more rapidly with increasing of sputtering time, which indicates that less or thinner SEI was formed on HfO_2 coated Si electrode.

6.5. Conclusion

HfO_2 coatings have been shown to be effective surface passivation layers on Si electrodes to prevent chemical degradation. As a highly insulating material, HfO_2 can

effectively block the electrons that are necessary for reducing the electrolyte. Comparing with other oxide coatings, we found HfO_2 to have a better stability under electrochemical cycling. In addition to previously recognized desirable properties of artificial SEIs, such electronic insulating, ionic conducting and mechanically “tough”, we show in this work that the chemical stability is also needed to achieve long the cycle life and shell life. We envision that this work will provide helpful guidelines to design better a-SEI for Li-ion cells.

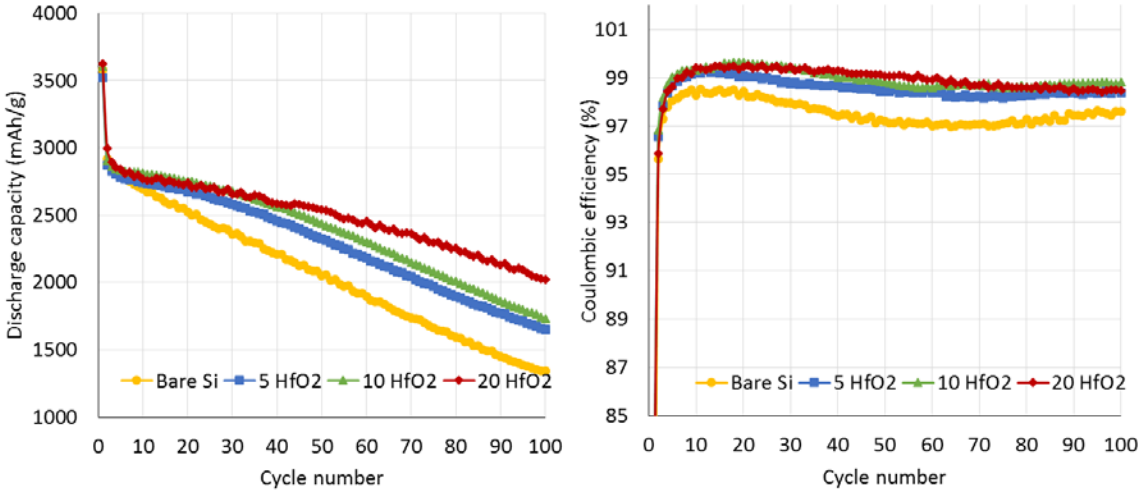

Figure 6.1 (Left) Discharge (lithiation) capacity (right) Coulombic efficiency of bare Si thin film electrodes, Si with 5/10/20 layers of HfO_2 coatings.

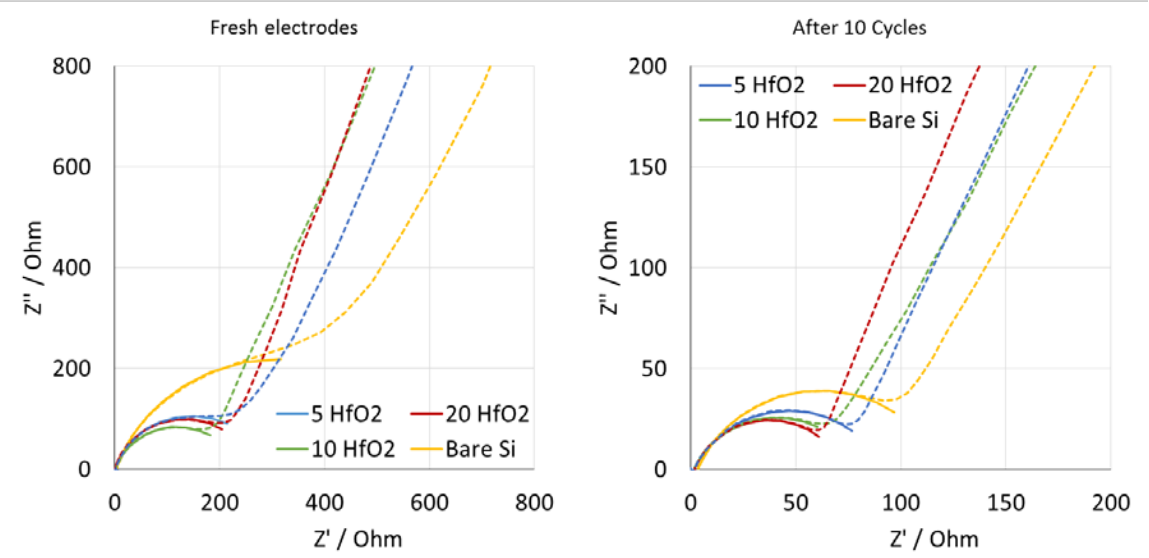

Figure 6.2 . Compare the EIS spectra for fresh and cycle-aged (10 cycles) electrodes The EIS spectra for cycle aged (10 cycles) with/without HfO2 coatings. EIS was measured under OCV.

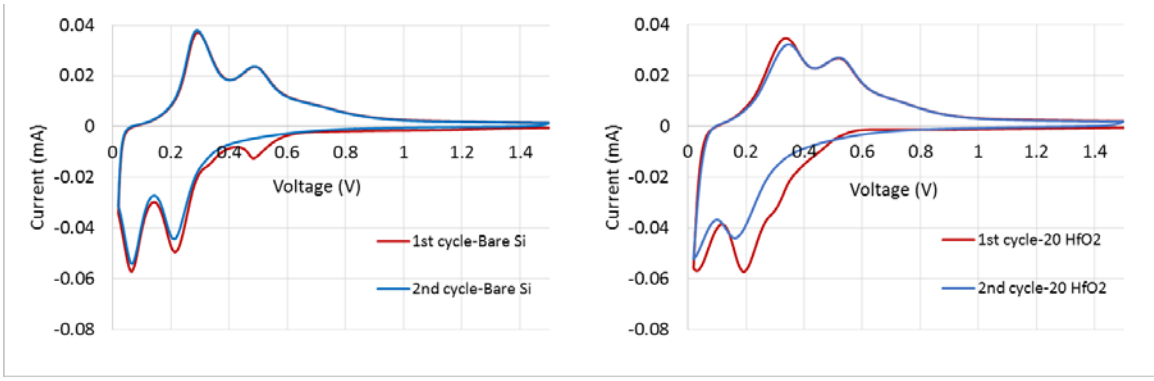

Figure 6.3 Cyclic voltammetry curves of bare Si electrodes (left) and Si coated with 20 layers of HfO2 (right)

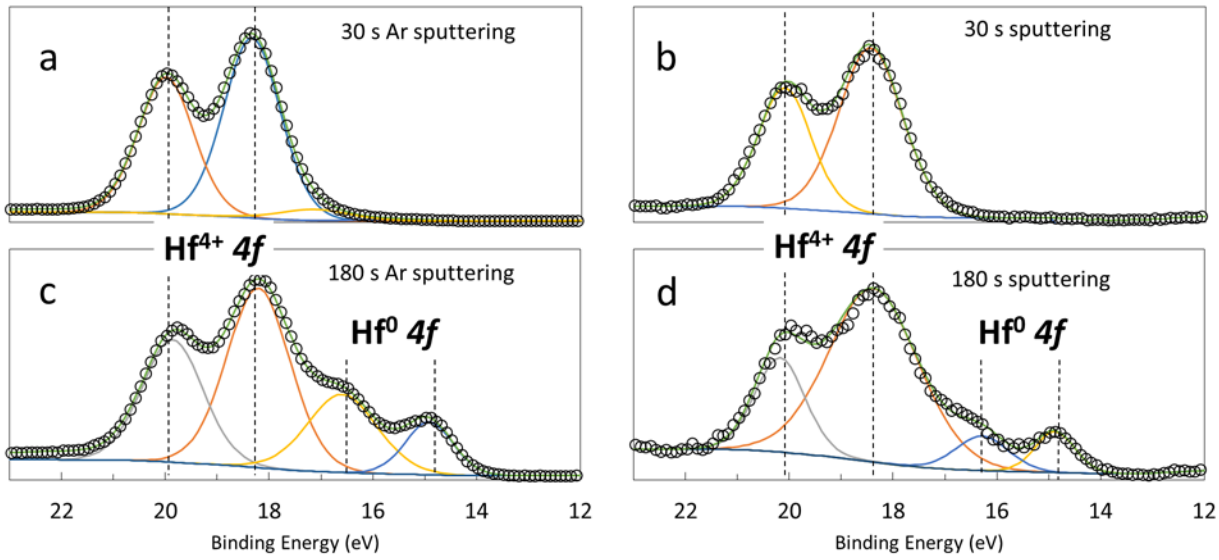

Figure 6.4 The Hf4f XPS spectra of the electrode surface before and after cycling; a and c: before cycling; b and d: after cycling (10 cycles)

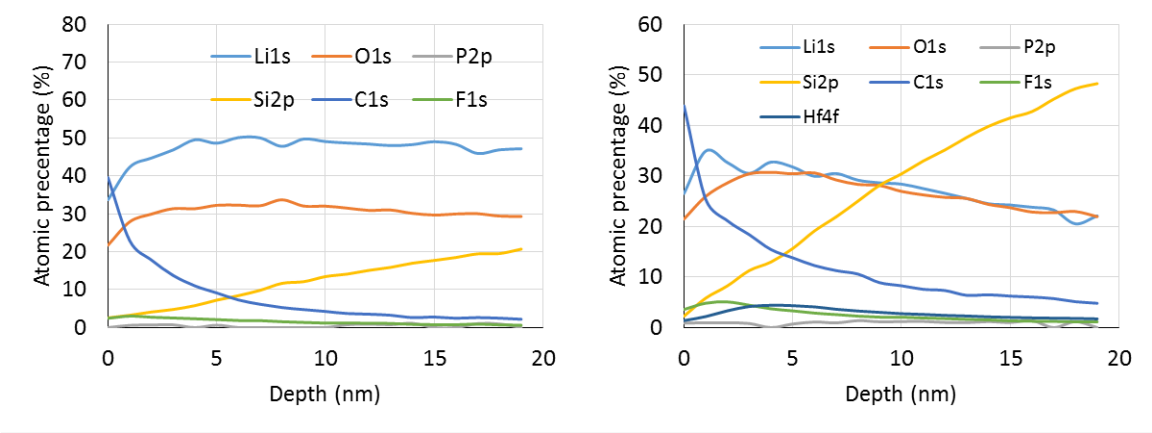

Figure 6.5 XPS depth profiles of bare Si electrode (left) and Si coated with 20 layers of HfO2 (right)

Table 6-1 Interfacial resistance (Rint) of electrodes with/without HfO2 coatings, fit from the semicircle of EIS measurements

	Fresh Electrode (Ohm)	**After 10 Cycles (Ohm)**
Bare Si	611.4	116.9
5 HFO_2	283.6	90.98
10 HFO_2	231.3	79.24
20 HFO_2	274.7	71.37

Chapter 7. Conclusion and Future Work

Surface coatings are essential for LIB positive electrodes, which can promote the electronic conductivity, or reduce the metal ion dissolution. While the LIB industry is trying to replace graphite electrodes with advanced anodes with greater Li ion storage capability. Anode coatings, or artificial SEIs, may be new industrial standard for LIBs.

We conclude that, the ideal coatings (artificial SEIs) should have four features:

(a) Electronic insulating (to reduce the formation of SEIs)
(b) Ionic conducting (to allow fast Li ion transport)
(c) Mechanically "strong" (to protect large strain electrodes)
(d) Chemically stable (to remain unchanged during cycling to reduce irreversible Li loss)

There is not a single general rule to guide the design of SEI, because different electrode materials require different levels of protection. For example, Si anode requires more mechanical protection, due to large volume change of this material during cycling. The selection of coating depends on its actual application. For example, the power battery requires large current during a short period of time (ionic conduction becomes more important); while the battery for medicinal devices requires longer calendar life (chemical stability becomes more important), etc. Depending on the systems and applications, one or more standards mentioned above are more critical than others.

The future directions for this topic should firstly be determining the limitations of current works. Most of the characterizations, especially the mechanical measurements, were carried out on the freshly made electrodes, or right after the formation cycle. However, the evolution of coatings, as well as the evolution of SEIs, should also be examined. The property change will continuously influence the performance of the electrode-coating systems.

Secondly, it will be interesting to see whether the conclusions presented in this dissertation can be tested on electrodes consisting micro- and nano-particles. In this research, thin-film electrode systems were used to facilitate the characterization of artificial/natural SEI. Some of the conclusions may be different if the coatings are applied to the surfaces of particle electrodes.

REFERENCE

1. Mizushima, K., et al., *LixCoO2 (0< x<-1): A new cathode material for batteries of high energy density.* Materials Research Bulletin, 1980. **15**(6): p. 783-789.
2. Li, X., et al., *Template-synthesized LiCoO2, LiMn2O4, and LiNi0. 8Co0. 2O2 nanotubes as the cathode materials of lithium ion batteries.* The Journal of Physical Chemistry B, 2005. **109**(29): p. 14017-14024.
3. Padhi, A.K., K. Nanjundaswamy, and J. Goodenough, *Phospho‐olivines as positive‐electrode materials for rechargeable lithium batteries.* Journal of the electrochemical society, 1997. **144**(4): p. 1188-1194.
4. Sun, C., et al., *Monodisperse porous LiFePO4 microspheres for a high power Li-ion battery cathode.* Journal of the American Chemical Society, 2011. **133**(7): p. 2132-2135.
5. Croce, F., et al., *A novel concept for the synthesis of an improved LiFePO4 lithium battery cathode.* Electrochemical and Solid-State Letters, 2002. **5**(3): p. A47-A50.
6. Ohzuku, T. and Y. Makimura, *Layered Lithium Insertion Material of LiNi1/2Mn1/2O2: A Possible Alternative to LiCoO2 for Advanced Lithium-Ion Batteries.* Chemistry Letters, 2001(8): p. 744-745.
7. Ohzuku, T. and Y. Makimura, *Layered Lithium Insertion Material of LiCo1/3Ni1/3Mn1/3O2 for Lithium-Ion Batteries.* Chemistry Letters, 2001(7): p. 642-643.
8. Wu, Y.-P., E. Rahm, and R. Holze, *Carbon anode materials for lithium ion batteries.* Journal of Power Sources, 2003. **114**(2): p. 228-236.
9. Yoshio, M., et al., *Effect of Carbon Coating on Electrochemical Performance of Treated Natural Graphite as Lithium‐Ion Battery Anode Material.* Journal of The Electrochemical Society, 2000. **147**(4): p. 1245-1250.
10. Yoshio, M., R.J. Brodd, and A. Kozawa, *Lithium-Ion Batteries*. Vol. 1. 2009: Springer.
11. Huggins, R., *Advanced batteries: materials science aspects*. 2009: Springer.
12. Megahed, S. and B. Scrosati, *Lithium-ion rechargeable batteries.* Journal of Power Sources, 1994. **51**(1-2): p. 79-104.
13. Peled, E., *THE ELECTROCHEMICAL-BEHAVIOR OF ALKALI AND ALKALINE-EARTH METALS IN NON-AQUEOUS BATTERY SYSTEMS - THE SOLID ELECTROLYTE INTERPHASE MODEL*. Journal of the Electrochemical Society, 1979. **126**(12): p. 2047-2051.
14. Paled, E., et al., *Lithium-Ion Batteries: Solid-Electrolyte Interphase*, 2004, College Press, London.
15. Cui, L.-F., et al., *Crystalline-amorphous core− shell silicon nanowires for high capacity and high current battery electrodes.* Nano Letters, 2008. **9**(1): p. 491-495.
16. Bourderau, S., T. Brousse, and D. Schleich, *Amorphous silicon as a possible anode material for Li-ion batteries.* Journal of power sources, 1999. **81**: p. 233-236.

17. Xiao, X., et al., *Improved cycling stability of silicon thin film electrodes through patterning for high energy density lithium batteries.* Journal of Power Sources, 2011. **196**(3): p. 1409-1416.
18. Christensen, J., *Modeling diffusion-induced stress in Li-ion cells with porous electrodes.* Journal of the Electrochemical Society, 2010. **157**(3): p. A366-A380.
19. Arora, P., R.E. White, and M. Doyle, *Capacity Fade Mechanisms and Side Reactions in Lithium‐Ion Batteries.* Journal of the Electrochemical Society, 1998. **145**(10): p. 3647-3667.
20. Lee, S.W., et al., *Fracture of crystalline silicon nanopillars during electrochemical lithium insertion.* Proceedings of the National Academy of Sciences, 2012. **109**(11): p. 4080-4085.
21. Liu, X.H., et al., *Anisotropic swelling and fracture of silicon nanowires during lithiation.* Nano letters, 2011. **11**(8): p. 3312-3318.
22. Liu, X.H., et al., *Size-dependent fracture of silicon nanoparticles during lithiation.* Acs Nano, 2012. **6**(2): p. 1522-1531.
23. Chan, C.K., et al., *High-performance lithium battery anodes using silicon nanowires.* Nature nanotechnology, 2008. **3**(1): p. 31-35.
24. Choi, N.-S., et al., *Effect of fluoroethylene carbonate additive on interfacial properties of silicon thin-film electrode.* Journal of Power Sources, 2006. **161**(2): p. 1254-1259.
25. Dalavi, S., P. Guduru, and B.L. Lucht, *Performance Enhancing Electrolyte Additives for Lithium Ion Batteries with Silicon Anodes.* Journal of The Electrochemical Society, 2012. **159**(5): p. A642-A646.
26. Yu, Y., et al., *Reversible Storage of Lithium in Silver‐Coated Three‐Dimensional Macroporous Silicon.* Advanced Materials, 2010. **22**(20): p. 2247-2250.
27. Yang, Y., et al., *New nanostructured Li2S/silicon rechargeable battery with high specific energy.* Nano letters, 2010. **10**(4): p. 1486-1491.
28. Xiao, X., P. Lu, and D. Ahn, *Ultrathin multifunctional oxide coatings for lithium ion batteries.* Advanced Materials, 2011. **23**(34): p. 3911-3915.
29. Dolle, M., et al., *In situ TEM study of the interface carbon/electrolyte.* Journal of power sources, 2001. **97**: p. 104-106.
30. Smart, M., et al., *Irreversible Capacities of Graphite in Low‐Temperature Electrolytes for Lithium‐Ion Batteries.* Journal of The Electrochemical Society, 1999. **146**(11): p. 3963-3969.
31. Gachot, G., et al., *Deciphering the multi-step degradation mechanisms of carbonate-based electrolyte in Li batteries.* Journal of Power Sources, 2008. **178**(1): p. 409-421.
32. Wu, H., et al., *Stable cycling of double-walled silicon nanotube battery anodes through solid-electrolyte interphase control.* Nature nanotechnology, 2012. **7**(5): p. 310-315.
33. Ulldemolins, M., et al., *Investigation on the part played by the solid electrolyte interphase on the electrochemical performances of the silicon electrode for lithium-ion batteries.* Journal of Power Sources, 2012. **206**: p. 245-252.

34. Lu, P., et al., *Chemistry, Impedance, and Morphology Evolution in SEI Films during Formation in Lithium Ion Batteries.* The Journal of Physical Chemistry C, 2013.
35. Zhang, S., et al., *Understanding solid electrolyte interface film formation on graphite electrodes.* Electrochemical and Solid-State Letters, 2001. **4**(12): p. A206-A208.
36. Elazari, R., et al., *Li ion cells comprising lithiated columnar silicon film anodes, TiS2 cathodes and fluoroethyene carbonate (FEC) as a critically important component.* Journal of The Electrochemical Society, 2012. **159**(9): p. A1440-A1445.
37. Etacheri, V., et al., *Effect of fluoroethylene carbonate (FEC) on the performance and surface chemistry of Si-nanowire Li-ion battery anodes.* Langmuir, 2011. **28**(1): p. 965-976.
38. Markevich, E., et al., *Amorphous Columnar Silicon Anodes for Advanced High Voltage Lithium Ion Full Cells: Dominant Factors Governing Cycling Performance.* Journal of The Electrochemical Society, 2013. **160**(10): p. A1824-A1833.
39. Chan, C.K., et al., *Surface chemistry and morphology of the solid electrolyte interphase on silicon nanowire lithium-ion battery anodes.* Journal of Power Sources, 2009. **189**(2): p. 1132-1140.
40. Nix, W.D., *Mechanical properties of thin films.* Metallurgical transactions A, 1989. **20**(11): p. 2217-2245.
41. Neubrand, A. and P. Hess, *Laser generation and detection of surface acoustic waves: Elastic properties of surface layers.* Journal of applied physics, 1992. **71**(1): p. 227-238.
42. Neubrand, A., L. Konstantinov, and P. Hess, *Interferometric probing of optically excited surface acoustic wave pulses for thin film characterization*, in *Physical Acoustics*. 1991, Springer. p. 551-556.
43. Limthongkul, P., et al., *Electrochemically-driven solid-state amorphization in lithium-silicon alloys and implications for lithium storage.* Acta Materialia, 2003. **51**(4): p. 1103-1113.
44. Kang, S.-H., et al., *Investigating the solid electrolyte interphase using binder-free graphite electrodes.* Journal of Power Sources, 2008. **175**(1): p. 526-532.
45. Bar‐Tow, D., E. Peled, and L. Burstein, *A Study of Highly Oriented Pyrolytic Graphite as a Model for the Graphite Anode in Li‐Ion Batteries.* Journal of The Electrochemical Society, 1999. **146**(3): p. 824-832.
46. Zhang, S., K. Xu, and T. Jow, *EIS study on the formation of solid electrolyte interface in Li-ion battery.* Electrochimica acta, 2006. **51**(8): p. 1636-1640.
47. Bauer, H. and W.P. Mason, *Physical Acoustics: Principles and Methods*. 1965: Academic Press.
48. Schneider, D. and T. Schwarz, *A photoacoustic method for characterising thin films.* Surface and Coatings Technology, 1997. **91**(1): p. 136-146.
49. Schneider, D., et al., *Non-destructive evaluation of diamond and diamond-like carbon films by laser induced surface acoustic waves.* Thin Solid Films, 1997. **295**(1): p. 107-116.

50. Schneider, D., et al., *Testing ultra-thin films by laser-acoustics.* Surface and Coatings Technology, 2000. **126**(2): p. 136-141.
51. Maznev, A.A., A. Akthakul, and K.A. Nelson, *Surface acoustic modes in thin films on anisotropic substrates.* Journal of applied physics, 1999. **86**(5): p. 2818-2824.
52. Thurston, E.b.W.P.M.a.R.N., *Physical Acoustics* 1972, New York.
53. Verma, P., P. Maire, and P. Novák, *A review of the features and analyses of the solid electrolyte interphase in Li-ion batteries.* Electrochimica Acta, 2010. **55**(22): p. 6332-6341.
54. Nie, M., et al., *Silicon solid electrolyte interphase (SEI) of lithium ion battery characterized by microscopy and spectroscopy.* The Journal of Physical Chemistry C, 2013. **117**(26): p. 13403-13412.
55. Leskelä, M. and M. Ritala, *Atomic layer deposition (ALD): from precursors to thin film structures.* Thin solid films, 2002. **409**(1): p. 138-146.
56. George, S.M., *Atomic layer deposition: an overview.* Chemical Reviews, 2009. **110**(1): p. 111-131.
57. Jones, A.C. and M.L. Hitchman, *Chemical vapour deposition: precursors, processes and applications*. 2009: Royal Society of Chemistry.
58. Frank, M.M., et al., *HfO 2 and Al 2 O 3 gate dielectrics on GaAs grown by atomic layer deposition.* Applied Physics Letters, 2005. **86**(15): p. 152904-152904-3.
59. Choi, B., et al., *Resistive switching mechanism of TiO2 thin films grown by atomic-layer deposition.* Journal of Applied Physics, 2005. **98**(3): p. 033715.
60. Yamada, A., B. Sang, and M. Konagai, *Atomic layer deposition of ZnO transparent conducting oxides.* Applied Surface Science, 1997. **112**: p. 216-222.
61. Hausmann, D.M., et al., *Atomic layer deposition of hafnium and zirconium oxides using metal amide precursors.* Chemistry of materials, 2002. **14**(10): p. 4350-4358.
62. King, J., et al., *High-filling-fraction inverted ZnS opals fabricated by atomic layer deposition*, 2003, DTIC Document.
63. Knez, M., K. Nielsch, and L. Niinistö, *Synthesis and surface engineering of complex nanostructures by atomic layer deposition.* Advanced Materials, 2007. **19**(21): p. 3425-3438.
64. Pilvi, T., et al., *Novel ALD process for depositing CaF2 thin films.* Chemistry of materials, 2007. **19**(14): p. 3387-3392.
65. Ylilammi, M. and T. Ranta‐aho, *Metal fluoride thin films prepared by atomic layer deposition.* Journal of The Electrochemical Society, 1994. **141**(5): p. 1278-1284.
66. Aaltonen, T., et al., *Atomic layer deposition of noble metals: Exploration of the low limit of the deposition temperature.* Journal of materials research, 2004. **19**(11): p. 3353-6658.
67. King, J.S., et al., *Ultralow loading Pt nanocatalysts prepared by atomic layer deposition on carbon aerogels.* Nano letters, 2008. **8**(8): p. 2405-2409.
68. Putkonen, M., et al., *Atomic layer deposition of polyimide thin films.* Journal of Materials Chemistry, 2007. **17**(7): p. 664-669.

69. Cho, M.-H., et al., *Thermal stability and structural characteristics of HfO 2 films on Si (100) grown by atomic-layer deposition.* Applied physics letters, 2002. **81**(3): p. 472-474.
70. Niinistö, L., et al., *Advanced electronic and optoelectronic materials by Atomic Layer Deposition: An overview with special emphasis on recent progress in processing of high‐k dielectrics and other oxide materials.* physica status solidi (a), 2004. **201**(7): p. 1443-1452.
71. Schmidt, J., et al., *Surface passivation of high‐efficiency silicon solar cells by atomic‐layer‐deposited Al2O3.* Progress in photovoltaics: research and applications, 2008. **16**(6): p. 461-466.
72. Hoex, B., et al., *Ultralow surface recombination of c-Si substrates passivated by plasma-assisted atomic layer deposited Al2O3.* Applied Physics Letters, 2006. **89**(4): p. 042112.
73. Elam, J., et al., *Conformal coating on ultrahigh-aspect-ratio nanopores of anodic alumina by atomic layer deposition.* Chemistry of Materials, 2003. **15**(18): p. 3507-3517.
74. Jiang, X., et al., *Application of atomic layer deposition of platinum to solid oxide fuel cells.* Chemistry of materials, 2008. **20**(12): p. 3897-3905.
75. Liu, C., et al., *Atomic Layer Deposition of Platinum Nanoparticles on Carbon Nanotubes for Application in Proton‐Exchange Membrane Fuel Cells.* Small, 2009. **5**(13): p. 1535-1538.
76. Elam, J., et al., *Improved nucleation of TiN atomic layer deposition films on SiLK low-k polymer dielectric using an Al2O3 atomic layer deposition adhesion layer.* Journal of Vacuum Science & Technology B, 2003. **21**(3): p. 1099-1107.
77. Jung, Y.S., et al., *Enhanced stability of LiCoO2 cathodes in lithium-ion batteries using surface modification by atomic layer deposition.* Journal of The Electrochemical Society, 2010. **157**(1): p. A75-A81.
78. Jung, Y.S., et al., *Ultrathin Direct Atomic Layer Deposition on Composite Electrodes for Highly Durable and Safe Li‐Ion Batteries.* Advanced Materials, 2010. **22**(19): p. 2172-2176.
79. Soni, S.K., et al., *Thickness effects on the lithiation of amorphous silicon thin films.* Scripta Materialia, 2011. **64**(4): p. 307-310.
80. Xiao, X., et al., *Lithium-ion batteries with coated separators*, 2013, Google Patents.
81. Tapily, K., et al., *Nanoindentation investigation of HfO2 and Al2O3 films grown by atomic layer deposition.* Journal of The Electrochemical Society, 2008. **155**(7): p. H545-H551.
82. Tripp, M.K., et al., *The mechanical properties of atomic layer deposited alumina for use in micro-and nano-electromechanical systems.* Sensors and Actuators A: Physical, 2006. **130**: p. 419-429.
83. Hickernell, T., F. Fliegel, and F. Hickernell. *The elastic properties of thin-film silicon nitride*. in *Ultrasonics Symposium, 1990. Proceedings., IEEE 1990*. 1990. IEEE.
84. Groner, M., et al., *Low-temperature Al2O3 atomic layer deposition.* Chemistry of Materials, 2004. **16**(4): p. 639-645.

85. Perevalov, T., et al., *Oxygen deficiency defects in amorphous Al 2 O 3.* Journal of Applied Physics, 2010. **108**(1): p. 013501-013501-4.
86. Alexander, J.F.S.W., *CRC Materials Science and Engineering Handbook.* Third Edition ed., New York: CRC Press
87. Petersen, K.E., *Silicon as a mechanical material.* Proceedings of the IEEE, 1982. **70**(5): p. 420-457.
88. Herrmann, C.F., et al. *Properties of atomic-layer-deposited Al2O3/ZnO dielectric films grown at low temperature for RF MEMS*. in *MOEMS-MEMS Micro & Nanofabrication*. 2005. International Society for Optics and Photonics.
89. Armand, M. and J.-M. Tarascon, *Building better batteries.* Nature, 2008. **451**(7179): p. 652-657.
90. Tarascon, J.-M. and M. Armand, *Issues and challenges facing rechargeable lithium batteries.* Nature, 2001. **414**(6861): p. 359-367.
91. Lee, J.K., et al., *Silicon nanoparticles–graphene paper composites for Li ion battery anodes.* Chemical Communications, 2010. **46**(12): p. 2025-2027.
92. Su, X., et al., *Silicon‐based nanomaterials for lithium‐ion batteries: a review.* Advanced Energy Materials, 2014. **4**(1).
93. Zhang, Q., et al., *Toward High Cycle Efficiency of Silicon‐Based Negative Electrodes by Designing the Solid Electrolyte Interphase.* Advanced Energy Materials, 2015. **5**(5).
94. Li, J., et al., *Atomic layered coating enabling ultrafast surface kinetics at silicon electrodes in lithium ion batteries.* The Journal of Physical Chemistry Letters, 2013. **4**(20): p. 3387-3391.
95. Tokranov, A., et al., *In situ atomic force microscopy study of initial solid electrolyte interphase formation on silicon electrodes for Li-ion batteries.* ACS applied materials & interfaces, 2014. **6**(9): p. 6672-6686.
96. Chen, Z., et al., *Role of surface coating on cathode materials for lithium-ion batteries.* Journal of Materials Chemistry, 2010. **20**(36): p. 7606-7612.
97. Li, X., et al., *Tin oxide with controlled morphology and crystallinity by atomic layer deposition onto graphene nanosheets for enhanced lithium storage.* Advanced Functional Materials, 2012. **22**(8): p. 1647-1654.
98. Pan, J., Y.T. Cheng, and Y. Qi, *General method to predict voltage-dependent ionic conduction in a solid electrolyte coating on electrodes.* Physical Review B, 2015. **91**(13).
99. Shi, S.Q., et al., *Direct Calculation of Li-Ion Transport in the Solid Electrolyte Interphase.* Journal of the American Chemical Society, 2012. **134**(37): p. 15476-15487.
100. Shi, S.Q., et al., *Defect Thermodynamics and Diffusion Mechanisms in Li2CO3 and Implications for the Solid Electrolyte Interphase in Li-Ion Batteries.* Journal of Physical Chemistry C, 2013. **117**(17): p. 8579-8593.
101. Deshpande, R., et al., *Battery cycle life prediction with coupled chemical degradation and fatigue mechanics.* Journal of The Electrochemical Society, 2012. **159**(10): p. A1730-A1738.
102. Xu, K., S. Zhang, and R. Jow, *Electrochemical impedance study of graphite/electrolyte interface formed in LiBOB/PC electrolyte.* Journal of Power Sources, 2005. **143**(1–2): p. 197-202.

103. Xu, K., S. Zhang, and T.R. Jow, *Formation of the graphite/electrolyte interface by lithium bis (oxalato) borate.* Electrochemical and solid-state letters, 2003. **6**(6): p. A117-A120.
104. Bar-Tow, D., E. Peled, and L. Burstein, *A study of highly oriented pyrolytic graphite as a model for the graphite anode in Li-ion batteries.* Journal of the Electrochemical Society, 1999. **146**(3): p. 824-832.
105. Kim, J.W. and H.G. Lee, *Thermal and carbothermic decomposition of Na2CO3 and Li(2)CO3.* Metallurgical and Materials Transactions B-Process Metallurgy and Materials Processing Science, 2001. **32**(1): p. 17-24.
106. Duan, Y.H. and D.C. Sorescu, *Density functional theory studies of the structural, electronic, and phonon properties of Li2O and Li2CO3: Application to CO2 capture reaction.* Physical Review B, 2009. **79**(1).
107. Arreaga-Salas, D.E., et al., *Progression of Solid Electrolyte Interphase Formation on Hydrogenated Amorphous Silicon Anodes for Lithium-Ion Batteries.* Journal of Physical Chemistry C, 2012. **116**(16): p. 9072-9077.
108. Chandrasekaran, R., et al., *Analysis of lithium insertion/deinsertion in a silicon electrode particle at room temperature.* Journal of the Electrochemical Society, 2010. **157**(10): p. A1139-A1151.
109. Pan, J., et al., *Effects of stress on lithium transport in amorphous silicon electrodes for lithium-ion batteries.* Nano Energy, 2015. **13**: p. 192-199.
110. Verbrugge, M.W., et al., *Experimental and Theoretical Characterization of Electrode Materials that Undergo Large Volume Changes and Application to the Lithium–Silicon System.* The Journal of Physical Chemistry C, 2015. **119**(10): p. 5341-5349.
111. Xu, J., Q. Zhang, and Y.-T. Cheng, *High Capacity Silicon Electrodes with Nafion as Binders for Lithium-Ion Batteries.* Journal of The Electrochemical Society, 2016. **163**(3): p. A401-A405.
112. Zhang, Q., et al., *Toward High Cycle Efficiency of Silicon-Based Negative Electrodes by Designing the Solid Electrolyte Interphase.* Advanced Energy Materials, 2015. **5**(5).
113. He, Y.-B., et al., *Effect of solid electrolyte interface (SEI) film on cyclic performance of Li4Ti5O12 anodes for Li ion batteries.* Journal of Power Sources, 2013. **239**: p. 269-276.
114. Herstedt, M., et al., *Characterisation of the SEI formed on natural graphite in PC-based electrolytes.* Electrochimica Acta, 2004. **49**(27): p. 4939-4947.
115. Klink, S., et al., *New Insights into SEI Formation in Lithium Ion Batteries: Inhomogeneous Distribution of Irreversible Charge Losses Across Graphite Electrodes.* 17th International Meeting on Lithium Batteries (Imlb 2014), 2014. **62**(1): p. 265-271.
116. Nie, M., et al., *Silicon Solid Electrolyte Interphase (SEI) of Lithium Ion Battery Characterized by Microscopy and Spectroscopy.* Journal of Physical Chemistry C, 2013. **117**(26): p. 13403-13412.
117. Pinson, M.B. and M.Z. Bazant, *Theory of SEI Formation in Rechargeable Batteries: Capacity Fade, Accelerated Aging and Lifetime Prediction.* Journal of the Electrochemical Society, 2013. **160**(2): p. A243-A250.

118. Yamaguchi, S., et al., *SEI Film Formation On Graphite Anode Surfaces In Lithium Ion Battery.* Molecular Crystals and Liquid Crystals Science and Technology Section a-Molecular Crystals and Liquid Crystals, 1998. **322**: p. 239-244.
119. Veith, G.M., et al., *Direct Determination of Solid-Electrolyte Interphase Thickness and Composition as a Function of State of Charge on a Silicon Anode.* The Journal of Physical Chemistry C, 2015.
120. Abe, K., et al., *Functional electrolytes: Synergetic effect of electrolyte additives for lithium-ion battery.* Journal of Power Sources, 2008. **184**(2): p. 449-455.
121. An, Y., et al., *The effects of LiBOB additive for stable SEI formation of PP13TFSI-organic mixed electrolyte in lithium ion batteries.* Electrochimica Acta, 2011. **56**(13): p. 4841-4848.
122. An, Y., et al., *Effects of VC-LiBOB binary additives on SEI formation in ionic liquid-organic composite electrolyte.* Rsc Advances, 2012. **2**(10): p. 4097-4102.
123. Cao Cuong, N., et al., *Roles of Fluorine-doping in Enhancing Initial Cycle Efficiency and SEI Formation of Li-, Al-cosubstituted Spinel Battery Cathodes.* Bulletin of the Korean Chemical Society, 2013. **34**(2): p. 384-388.
124. Chen, W., et al., *Study of the formation of a solid electrolyte interphase (SEI) in ionically crosslinked polyampholytic gel electrolytes.* Electrochimica Acta, 2008. **53**(13): p. 4414-4419.
125. Etacheri, V., et al., *Effect of Fluoroethylene Carbonate (FEC) on the Performance and Surface Chemistry of Si-Nanowire Li-Ion Battery Anodes.* Langmuir, 2012. **28**(1): p. 965-976.
126. Ganesh, P., P.R.C. Kent, and D.-e. Jiang, *Solid-Electrolyte Interphase Formation and Electrolyte Reduction at Li-Ion Battery Graphite Anodes: Insights from First-Principles Molecular Dynamics.* Journal of Physical Chemistry C, 2012. **116**(46): p. 24476-24481.
127. Park, Y., et al., *Investigation of solid electrolyte interface (SEI) film on LiCoO2 cathode in fluoroethylene carbonate (FEC)-containing electrolyte by 2D correlation X-ray photoelectron spectroscopy (XPS).* Journal of Molecular Structure, 2014. **1069**: p. 157-163.
128. Fu, L.J., et al., *Surface modifications of electrode materials for lithium ion batteries.* Solid State Sciences, 2006. **8**(2): p. 113-128.
129. Schroder, K.W., et al., *Role of Surface Oxides in the Formation of Solid-Electrolyte Interphases at Silicon Electrodes for Lithium-Ion Batteries.* Acs Applied Materials & Interfaces, 2014. **6**(23): p. 21510-21524.
130. Li, J., et al., *Artificial Solid Electrolyte Interphase To Address the Electrochemical Degradation of Silicon Electrodes.* Acs Applied Materials & Interfaces, 2014. **6**(13): p. 10083-10088.
131. Meng, X., X.Q. Yang, and X. Sun, *Emerging Applications of Atomic Layer Deposition for Lithium‐Ion Battery Studies.* Advanced Materials, 2012. **24**(27): p. 3589-3615.
132. Zhang, Q., et al., *A non-destructive method for measuring the mechanical properties of ultrathin films prepared by atomic layer deposition.* Applied Physics Letters, 2014. **105**(6): p. 061901.

133. Wang, H.-Y. and F.-M. Wang, *Electrochemical investigation of an artificial solid electrolyte interface for improving the cycle-ability of lithium ion batteries using an atomic layer deposition on a graphite electrode.* Journal of Power Sources, 2013. **233**: p. 1-5.
134. Hy, S., et al., *In situ surface enhanced Raman spectroscopic studies of solid electrolyte interphase formation in lithium ion battery electrodes.* Journal of Power Sources, 2014. **256**: p. 324-328.
135. Li, C., et al., *Cathode materials modified by surface coating for lithium ion batteries.* Electrochimica Acta, 2006. **51**(19): p. 3872-3883.
136. Lee, B.H., et al., *Thermal stability and electrical characteristics of ultrathin hafnium oxide gate dielectric reoxidized with rapid thermal annealing.* Applied Physics Letters, 2000. **76**(14): p. 1926-1928.
137. Cho, M.-H., et al., *Thermal stability and structural characteristics of HfO2 films on Si (100) grown by atomic-layer deposition.* Applied physics letters, 2002. **81**: p. 472-474.
138. Han, L., et al., *Atomic Layer Deposition of High Quality HfO2 Using In-Situ Formed Hydrophilic Oxide as an Interfacial Layer.* ECS Journal of Solid State Science and Technology, 2014. **3**(12): p. N155-N160.
139. Hackley, J.C., J.D. Demaree, and T. Gougousi, *Growth and interface of HfO2 films on H-terminated Si from a TDMAH and H2O atomic layer deposition process.* Journal of Vacuum Science & Technology A, 2008. **26**(5): p. 1235-1240.
140. Hackley, J.C. and T. Gougousi, *Properties of atomic layer deposited HfO< sub> 2</sub> thin films.* Thin Solid Films, 2009. **517**(24): p. 6576-6583.
141. Ho, M.-T., et al., *In situ infrared spectroscopy of hafnium oxide growth on hydrogen-terminated silicon surfaces by atomic layer deposition.* Applied Physics Letters, 2005. **87**(13): p. 133103-133103-3.
142. Li, K., et al., *Tetrakis (dimethylamido) hafnium adsorption and reaction on hydrogen terminated Si (100) surfaces.* The Journal of Physical Chemistry C, 2010. **114**(33): p. 14061-14075.
143. Christensen, J. and J. Newman, *Effect of anode film resistance on the charge/discharge capacity of a lithium-ion battery.* Journal of the Electrochemical Society, 2003. **150**(11): p. A1416-A1420.
144. Lu, B., et al., *Voltage hysteresis of lithium ion batteries caused by mechanical stress.* Physical Chemistry Chemical Physics, 2016.
145. Filatova, E., et al., *XPS and depth resolved SXES study of HfO 2/Si interlayers.* Journal of Electron Spectroscopy and Related Phenomena, 2010. **181**(2): p. 206-210.
146. Aurbach, D., *Review of selected electrode–solution interactions which determine the performance of Li and Li ion batteries.* Journal of Power Sources, 2000. **89**(2): p. 206-218.

VITA

Qinglin Zhang was born in 1989 in Harbin, Heilongjiang Province, P. R. China.

EDUCATION

B. Eng., Materials Science and Engineering, Northwestern Polytechnical University
Xi'an, China 2011

Graduate Certificate in Power and Energy, Power and Energy Institute of Kentucky
Fall, 2012

PROFESSIONAL AFFILIATIONS AND SERVICES

Student member, Materials Research Society (MRS)	Since 2012
President, MRS-UK Chapter	2014-2016
Student member, Electrochemical Society (ECS)	Since 2012
Vice president, ECS-Kentucky Chapter	2015
Student member, ASM International	Since 2014

AWARDS AND INVITED TALKS

Outstanding Graduate Student Award on *Improving the capacity, durability and stability of Li-ion batteries* Department of Chemical and Materials Engineering, University of Kentucky 2015

Best Student Oral Presentation Award Materials Research Society 2015 Fall Meeting, Boston 2015

Invited talk *"Silicon Electrode and the Interphases"*, Shanghai University 2015

Northwestern Polytechnical University Scholarship 2010

PUBLICATIONS (Updated Feb. 2016)

Lithium-ion battery

Qinglin Zhang, Jie Pan, Peng Lu, Mark W Verbrugge, Brain W Shelton, Yang-Tse Cheng, Yue Qi and Xingcheng Xiao, "Synergetic Effects of Inorganic Components in Solid Electrolyte In-terphase on High Cycle Efficiency of Lithium Ion Batteries," ***Nano Letters***, 16 (3) : 2011-2016 (2016)

Jie Pan, **Qinglin Zhang**, Xingcheng Xiao, Yang-Tse Cheng and Yue Qi, "Design of Nano-Structured Heterogeneous Solid Ionic Coatings for Lithium Ion Batteries through a Multi-Scale Defect Model," ***ACS Applied Materials & Interfaces***, 8 (8) : 5687-5693 (2016)

Tao Chen, **Qinglin Zhang**, Jiagang Xu, Jie Pan and Yang-Tse Cheng, "A Binder-Free Si Based Anode for Li-Ion Batteries from Lignin," submitted to ***RSC Advances***

Jiagang Xu, **Qinglin Zhang**, Yang-Tse Cheng, "High capacity silicon electrodes with Nafion as binders for lithium-ion batteries," ***Journal of Electrochemical Society***, 163 (3), A401-A405

Juchuan Li, **Qinglin Zhang**, Xingcheng Xiao, Yang-Tse Cheng, Chengdu Liang, Nancy J Dudney, "Unravelling the Impact of Reaction Paths on Mechanical Degradation of Intercalation Cathodes for Lithium-Ion Batteries," ***Journal of the American Chemical Society***, 137 (43) : 13732-13735 (2015)

Qinglin Zhang, Xingcheng Xiao, Weidong Zhou, Yang-Tse Cheng and Mark W. Verbrugge. "Towards High Cycle Efficiency of Silicon-Based Negative Electrodes by Designing Solid Electrolyte Interphase," ***Advanced Energy Materials***, 5 (5) : 1401398 (2015)

Jie Pan, **Qinglin Zhang**, Juchuan Li, Matthew Beck, Xingcheng Xiao and Yang-Tse Cheng, "Effects of Stress on Lithium Transport in Amorphous Silicon Electrodes for Lithium-ion Batteries," ***Nano Energy***, 13, 192-199, (2015)

Mark Verbrugge, Daniel Baker, Xingcheng Xiao, **Qinglin Zhang** and Yang-Tse Cheng, "Experimental and Theoretical Characterization of Electrode Materials that Undergo Large Volume Changes and Application to the Lithium-Silicon System, " ***Journal of Physical Chemical C***, 119 (10) : 5341-5349 (2015)

Qinglin Zhang, Xingcheng Xiao, Yang-Tse Cheng, and Mark W Verbrugge. "A non-destructive method for measuring the mechanical properties of ultrathin films prepared by atomic layer deposition," ***Applied Physics Letters***, 105(6) : 061901 (2014)

Mahendra K. Sreeramoju, John P. Selegue, **Qinglin Zhang**, and Yang-Tse Cheng. "Nanodiamond-derived carbon nano-onions as negative electrode materials for lithium-ion batteries." ***In Abstracts Of Papers of the American Chemical Society***, vol. 245. 1155 (2013)

Beyond Li-ion

Jianfeng Huang, Zhanwei Xu, Liyun Cao, **Qinglin Zhang**, Haibo Ouyang, Jiayin Li. Tailor MoO2/Graphene Oxide Nanoarchitectures for Stable and High Density Sodium Ion Anodes. ***Energy Technology***, 3 (11) : 1108-1114 (2015)

Weidong Zhou, Chongmin Wang, **Qinglin Zhang**, Héctor D. Abruña, Yang He, Jiangwei Wang, Scott X. Mao and Xingcheng Xiao, "Tailoring Pore Size of Nitrogen-Doped Hollow Carbon Nanospheres for Confining Sulfur in Lithium-Sulfur Batteries, " ***Advanced Energy Materials***, 5 (16) : 1401752 (2015)

Nanostructured Material Synthesis and Fuel Cell Catalyst

Zhanwei Xu, Hejun Li, Wei Li, Gaoxiang Cao, **Qinglin Zhang**, Kezhi Li, Qiangang Fu and Jie Wang. "Large-scale production of graphene by microwave synthesis and rapid cooling," ***Chemical Communications***, 47(4) : 1166-1168 (2011)

Hejun Li, Zhanwei Xu, Kezhi Li, Xianghui Hou, Gaoxiang Cao, **Qinglin Zhang** and Zeyuan Cao. "Modification of multi-walled carbon nanotubes with cobalt phthalocyanine: effects of the templates on the assemblies," ***Journal of Materials Chemistry***, 41 (4) : 1181-1186 (2011)

Qinglin Zhang, Zhanwei Xu, Hejun Li, Liyan Wu, Gaoxiang Cao and Kezhi Li. "Synthesis of MoS2 Nanosheets by Solid-State Reaction in CVD Furnace," ***Integrated Ferroelectrics***, 128 (1) : 125-129 (2011)

Zhanwei Xu, Hejun Li, Gaoxiang Cao, **Qinglin Zhang**, Kezhi Li, Xueni Zhao. "Electrochemical performance of carbon nanotube-supported cobalt phthalocyanine and its nitrogen-rich derivatives for oxygen reduction," ***Journal of Molecular Catalysis A: Chemical***, 335(1-2) : 89-96 (2011)

Zhanwei Xu, Hejun Li, Huijuan Luo, Huihui Sun, **Qinglin Zhang**, Gaoxiang Cao, Kezhi Li. "Graphite nanosheets doped with Fe, Ni, and N, synthesized in one step, and their unique magnetic performance," ***Solid State Communications***, 151(8) : 643-646 (2011)

Zhanwei Xu, Hejun Li, Huihui Sun, **Qinglin Zhang**, Kezhi Li. "Carbon Nanotubes with Phthalocyanine-Decorated Surface Produced by NH3-Assisted Microwave Reaction and Their Catalytic Performance in Li/SOCl2 Battery," ***Chinese Journal of Chemistry***, 28(10) : 2059-2066 (2010)

Zhanwei Xu, Hejun Li, Gaoxiang Cao, Zeyuan Cao, **Qinglin Zhang**, Kezhi Li, Xianghui Hou, Wei Li and Weifeng Cao. "Synthesis of hybrid graphene carbon-coated nanocatalysts," ***Journal of Materials Chemistry***, 38 (20) : 8230-8232 (2010)

Semiconductor and thin film

Xiaobai Yu, Xiaoxin Wang, **Qinglin Zhang**, and Jifeng Liu. "Interfacial Engineering of Solution-Processed Ni Nanochain-SiOx (x<2) Cermets towards Thermodynamically Stable, Anti-oxidation Solar Selective Absorbers," submitted to ***Journal of Applied Physics***

Lei Han, Jie Pan, **Qinglin Zhang**, Shibin Li and Zhi Chen. "Atomic Layer Deposition of High Quality HfO2 Using In-Situ Formed Hydrophilic Oxide as an Interfacial Layer," ***ECS Journal of Solid State Science and Technology***, 12(3) : N155-N160 (2014)

Xiaobai Yu, Xiaoxin Wang, **Qinglin Zhang**, Juchuan Li and, Jifeng Liu. "Oxidation-resistant, solution-processed plasmonic Ni nanochain-SiOx (x < 2) selective solar thermal absorbers," ***Journal of Applied Physics***, 116 (7) : 073508 (2014)

TECHNICAL PRESENTATIONS

Qinglin Zhang, Xingcheng Xiao, Yang-Tse Cheng and Mark Verbrugge, "Tailoring the composition of solid-electrolyte interphase for high efficiency silicon negative electrodes," 2015 MRS Fall Meeting, Boston, MA, 12/2015 (Abstract No. LL7.03, oral presentation)

Jiagang Xu, **Qinglin Zhang**, and Yang-Tse Cheng, "High Capacity Silicon Electrodes with Nafion as Binders, " *227th ECS Meeting*, Chicago, IL, 5/2015

Mark W. Verbrugge, Denial R. Baker, Xingcheng Xiao, **Qinglin Zhang**, and Yang-Tse Cheng, "Experimental and Theoretical Characterization of Electrode Materials That Undergo Large Volume Changes and Application to the Lithium-Silicon System," *227th ECS Meeting*, Chicago, IL, 5/2015 (Abstract #45144)

Yang-Tse Cheng, **Qinglin Zhang**, Mark Verbrugge and Xingcheng Xiao, "Understanding and Mitigating Coupled Mechanical-Chemical Degradation for Improving the Performance and Durability of Lithium Ion Batteries," 2015 MRS Spring Meeting, San Francisco, CA, 4/2015 (Abstract No. H1.05)

Qinglin Zhang, Yang-Tse Cheng, Xingcheng Xiao and Mark Verbrugge, "Towards High Cycle Efficiency of Silicon-Based Negative Electrodes by Designing Solid Electrolyte Interphase," *2015 MRS Spring Meeting*, San Francisco, CA, 4/2015 (Abstract No. I4.05, oral presentation)

Qinglin Zhang, Yang-Tse Cheng, Xingcheng Xiao and Mark Verbrugge, "Novel Techniques to Determine Mechanical Properties for Lithium Ion Batteries," The 40th annual American Vacuum Society - Michigan Chapter Symposium - Thin films for Energy Storage and Conversion Applications, East Lansing, MI, 2014. (Poster)

Qinglin Zhang and Yang-Yse Cheng, "Studies of Thin Coatings for Improving the Performance and Durability of Lithium Ion Batteries, " *2014 MS&T 14'*, Pittsburg, PA, 10/2014 (oral presentation)

Qinglin Zhang, Xingcheng Xiao, Yang-Tse Cheng and Mark Verbrugge. "Mechanical Properties of Solid-Electrolyte Interphase and Impact on Cycle Efficiency of Silicon-Based Negative Electrodes for Lithium Ion Batteries," *2014 MRS Fall Meeting*, Boston, MA, 12/2014 (Abstract No. Z4.09, oral presentation)